Universidade do Minho
Escola de Engenharia

Aritz Markes Larrinaga

Validation of an Interlaminar Damage Model Towards the Simulation of Large Structures

FRP++
Advanced structural analysis and design using composite materials

Funded by the European Union

August 2026

Validation of an Interlaminar Damage Model Towards the Simulation of Large Structures
Aritz Markes Larrinaga
FRP++ Advanced structural analysis and design using composite materials
UMinho | 2026

The European Master in Advanced Structural Analysis and Design using Composite Materials is a join initiative of:
Universidade do Minho · Universitat de Girona · Università degli Studi di Napoli Federico II · INSA Institut National des Sciences Appliquées Toulouse · Université de Toulouse

Universidade do Minho
Escola de Engenharia

Aritz Markes Larrinaga

Validation of an Interlaminar Damage Model Towards the Simulation of Large Structures

FRP++
Advanced structural analysis and design using composite materials

Master Dissertation
European Master Advanced Structural Analysis and Design using Composite Materials

Work developed under the supervision of
Professor Doctor Vítor Cunha
Professor Doctor Pere Maimi

Funded by the European Union

August 2026

DIREITOS DE AUTOR E CONDIÇÕES DE UTILIZAÇÃO DO TRABALHO POR TERCEIROS

Este é um trabalho académico que pode ser utilizado por terceiros desde que respeitadas as regras e boas práticas internacionalmente aceites, no que concerne aos direitos de autor e direitos conexos.

Assim, o presente trabalho pode ser utilizado nos termos previstos na licença abaixo indicada.

Caso o utilizador necessite de permissão para poder fazer um uso do trabalho em condições não previstas no licenciamento indicado, deverá contactar o autor, através do RepositóriUM da Universidade do Minho.

Licença concedida aos utilizadores deste trabalho



Atribuição-NãoComercial-SemDerivações CC BY-NC-ND

https://creativecommons.org/licenses/by-nc-nd/4.0/

ACKNOWLEDGEMENTS

I would like to express my sincere gratitude to my supervisors, Dr. Pere Maimí and Dr. Vítor Cunha, for their continuous guidance, valuable advice, and constructive feedback throughout this dissertation. Their expertise, encouragement, and support have been fundamental to the successful completion of this work. Their willingness to share their knowledge and provide insightful discussions has greatly contributed to both the technical quality of this research and my development as an engineer.

I would also like to express my special thanks to Pierre Daniel for his invaluable support throughout the development of the Adaptive ERR–Cohesive Large-Element Model. His patience in explaining the underlying methodology, his guidance in learning how to implement and use the user-defined subroutine, and his continuous assistance during the development and validation of the numerical model were essential to the completion of this dissertation. His expertise, availability, and willingness to answer countless technical questions enabled me to gain a much deeper understanding of the Adaptive ERR–Cohesive formulation and its practical implementation in LS-DYNA.

I would also like to thank the academic staff of the University of Girona and the University of Minho for providing an excellent learning environment throughout the Erasmus Mundus FRP++ programme. The opportunity to work within an international academic collaboration has been an invaluable experience that has significantly contributed to both my academic and personal development.

I would also like to gratefully acknowledge the financial support provided by the European Union for participation in the Erasmus Mundus FRP++ European Master Course in Advanced Structural Analysis and Design using Composite Materials (Project no. 101048961). This work was also supported by FCT/MCTES under the R&D Unit Institute for Sustainability and Innovation in Structural Engineering (ISISE), under the references UID/4029/2025 (DOI: 10.54499/UID/04029/2025), UID/PRR/04029/2025 (DOI: 10.54499/UID/PRR/04029/2025), and UID/PRR2/04029/2025 (DOI: 10.54499/UID/PRR2/04029/2025), and under the Associate Laboratory Advanced Production and Intelligent Systems ARISE under reference LA/P/0112/2020 (DOI: 10.54499/LA/P/0112/2020).

STATEMENT OF INTEGRITY

I hereby declare having conducted this academic work with integrity. I confirm that I have not used plagiarism or any form of undue use of information or falsification of results along the process leading to its elaboration.

I further declare that I have fully acknowledged the Code of Ethics and Conduct of the University of Minho.

DECLARATION ON THE USE OF ARTIFICIAL INTELLIGENCE (AI) TOOLS

I hereby declare having acted this academic work with integrity and confirm that I have not resorted to any form of undue use of AI tools, nor to the falsification or omission of information, sources, data, results or processes in any of the stages leading to its elaboration.

I further declare that any use of AI tools was done in a transparent and responsible manner, being duly noted in the work, and that I critically verified the accuracy of the content produced with their support, assuming full responsibility for what I submit.

I further declare that I have fully acknowledged the Code of Ethics and Conduct of the University of Minho, as well as the applicable standards of academic integrity and data protection.

Validação de um Modelo de Dano Interlaminar Orientado para a Simulação de Grande Dimensão

RESUMO

O grupo AMADE possui uma vasta experiência no desenvolvimento de modelos constitutivos para materiais compósitos capazes de representar diferentes mecanismos de dano. Recentemente, através de uma colaboração entre a B-Tech e a Universidade de Chalmers, foi desenvolvido um método número eficiente para a modelação do dano interlaminar (delaminação) com vista à aplicação em estruturas compósitas de grande dimensão.

O objetivo deste trabalho é validar um modelo numérico de dano interlaminar baseado numa formulação híbrida que combina critérios de taxa de libertação de energia (ERR) com elementos coesivos, permitindo a simulação eficiente da propagação da delaminação com malhas relativamente grosseiras. O modelo será aplicado à simulação de impacto de baixa velocidade numa estrutura compósita, de forma a avaliar a sua capacidade preditiva e a sua eficiência computacional em condições representativas de aplicações de engenharia à escala real.

A metodologia baseia-se principalmente em simulações numéricas recorrendo ao método dos elementos finitos. O modelo de dano interlaminar proposto é implementado numa simulação representativa de impacto de baixa velocidade e os resultados obtidos são comparados com um modelo numérico de referência previamente validado experimentalmente e descrito na literatura. Esta comparação permite avaliar a capacidade preditiva, a precisão e a eficiência computacional da abordagem proposta.

Este estudo pretende avaliar o potencial desta abordagem como uma ferramenta eficiente para a simulação de dano interlaminar em estruturas compósitas complexas. O trabalho será desenvolvido em colaboração entre AMADE e B-Tech, com uma componente predominantemente numérica (cerca de 90%) e uma componente analítica complementar (cerca de 10%).

PALAVRAS-CHAVE: Dano interlaminar 1; Impacto 2; Materiais compósitos 3; Estruturas de grande dimensão 4; Método dos elementos finitos (MEF) 5.

Validation of an Interlaminar Damage Model Towards the Simulation of Large Structures

ABSTRACT

AMADE has extensive experience in the development of constitutive models for composite materials capable of representing different damage mechanisms. Recently, through a collaboration between B-Tech and Chalmers University of Technology, an efficient numerical approach for modelling interlaminar damage (delamination) has been developed for application to large-scale composite structures.

The objective of this thesis is to validate a numerical interlaminar damage model based on a hybrid formulation that combines Energy Release Rate (ERR) criteria with cohesive elements, enabling the efficient simulation of delamination propagation using relatively coarse finite element meshes. The model is applied to the simulation of a low-velocity impact on a composite structure in order to evaluate its predictive capability and computational efficiency under conditions representative of real engineering applications.

The methodology is primarily based on finite element simulations. The proposed interlaminar damage model is implemented in a representative low-velocity impact simulation, and the obtained results are compared with those of a reference numerical model previously validated against experimental data and reported in the literature. This comparison allows the predictive capability, accuracy, and computational efficiency of the proposed approach to be assessed.

This study aims to evaluate the potential of the proposed approach as an efficient tool for simulating interlaminar damage in complex composite structures. The work is carried out in collaboration with AMADE and B-Tech and consists predominantly of numerical simulations, complemented by a smaller analytical component.

KEYWORDS: Interlaminar damage 1; Impact 2; Composite Materials 3; Large-Scale structures 4; Numerical validation 5.

TABLE OF CONTENTS

Acknowledgements iii
Validação de um Modelo de Dano Interlaminar Orientado para a Simulação de Grande Dimensão v
Resumo v
Validation of an Interlaminar Damage Model Towards the Simulation of Large Structures vi
Abstract vi
Table of Contents vii
List of Figures x
List of Tables xiii
List of Abbreviations and Symbols xiv
1. Introduction 1
1.1. Motivation 2
1.2. Objectives 3
1.3. Structure of the dissertation 5
2. Literature Review 7
2.1. Energy Release Rate Methods for Delamination Modelling 8
2.1.1. Virtual Crack Closure Technique 10
2.1.2. Efficiency of VCCT for Large Structural Models 13
2.1.3. Limitations of VCCT 14
2.1.4. Progressive Node Release Methods 14
2.2. Cohesive Zone Models for Delamination 16
2.2.1. Fundamentals 16
2.2.2. Damage Initiation Criteria 18
2.2.3. Damage Evolution Laws 20
2.2.4. Advantages and Limitations of CZM 22
2.3. Hybrid ERR–Cohesive Approaches for Delamination Modelling 24
2.3.1. Motivation for Hybrid Formulations 24
2.3.2. ERR–Cohesive Formulation 25

2.3.3. Application to Large Structural Models 27
2.3.4. Extension to Arbitrary Delamination Fronts 30
2.4. Critical Comparison of Delamination Modelling Approaches 31
3. METHODOLOGY 33
3.1. Experimental Programme 33
3.1.1. Standard and Reference Study 33
3.1.2. Specimen Geometry and Laminate Configuration 34
3.1.3. Material and Mechanical Properties 35
3.1.4. Test Setup 37
3.1.5. Validation Criteria and Experimental Reference Results 37
3.2. Layer-wise Model with Cohesive Interfaces (Abaqus®) 38
3.2.1. Model Overview 38
3.2.2. Element and Mesh Discretization 39
3.2.3. Laminate Constitutive Modelling 40
3.2.4. Intralaminar Damage Modelling 42
3.2.5. Cohesive Interface Modelling 48
3.2.6. Contact Interactions 49
3.2.7. Boundary and Load Conditions 50
3.2.8. Output Requests 50
3.2.9. Model Calibration 51
3.3. Adaptive ERR-Cohesive Large Element Model (LS-DYNA®) 52
3.3.1. Laminate Material Definition 52
3.3.2. Model Organisation 52
3.3.3. Mesh Discretization 54
3.3.4. Adaptive Delamination Parameters 55
3.3.5. Intralaminar Damage Modelling 56
3.3.6. Output Requests 58
4. Results and Discussion 61
4.1. Validation Strategy and Scope 61
4.2. Initial Elastic Response Validation 61

4.3. Layer-wise Model with Cohesive Interface Behaviour and Intralaminar Damage .. 65
4.3.1. Force–displacement response 65
4.3.2. Energy response 67
4.3.3. Delamination prediction 71
4.4. Adaptive ERR–Cohesive Large-Element Model Results 73
4.4.1. Global Structural Response 73
4.4.2. Hourglass Stiffness Sensitivity 76
4.4.3. Influence of the Enriched Interface Configuration 78
4.4.4. Delamination Pattern Validation 80
4.5. Comparative Assessment of the Two Modelling Approaches 82
4.5.1. Validated aspects 82
4.5.2. Limitations 83
4.5.3. Suitability for large-scale structures 84
5. Conclusions 87
5.1. Summary of the main findings 87
5.2. Research Objectives Achievement 89
5.3. Limitations and Future Work 90
References 92

LIST OF FIGURES

Figure 1.1 Framework for multiscale modelling of delamination in composite structures (after Daniel [16]) 4
Figure 2.1 Schematic representation of the three fundamental delamination fracture modes in laminated composites: Mode I (opening), Mode II (sliding) and Mode III (tearing). Adapted from Hull and Clyne [2]. 9
Figure 2.2 Schematic representation of the Crack Closure Technique used to compute the energy release rate [16]. 11
Figure 2.3 Schematic representation of the crack-tip configuration in the VCCT method [16]. 12
Figure 2.4 Traction–separation law for a cohesive interface element showing elastic behaviour, damage initiation and progressive stiffness degradation until complete separation [25]. 17
Figure 2.5 Traction–separation relationships for pure loading modes in cohesive interface models: (a) shear loading (mode II/III) and (b) opening loading (mode I), taken from Camanho et al. [7]. 18
Figure 2.6 Bilinear traction–separation law describing damage initiation and evolution in cohesive zone models (taken from Turon et al. [28]). 21
Figure 2.7 Adaptive enrichment strategy proposed by Daniel [16]. 25
Figure 2.8 Crack-tip configuration employed by the adaptive ERR–cohesive formulation (adapted from Daniel et al. [11]). 26
Figure 2.9 Comparison of delamination propagation predicted using conventional cohesive elements and the proposed method with larger finite elements (after Daniel et al. [10]). ... 28
Figure 2.10 Force–displacement response obtained with the proposed large-element approach compared with the analytical solution and a fine-mesh cohesive zone model. Taken from Daniel et al. [10]. 29
Figure 3.1 Test Configuration Setup 33
Figure 3.2 Top View Dimensions. All dimensions are in mm. 35
Figure 3.3 Lateral View Dimensions. All dimensions are in mm. 35
Figure 3.4 Base Opening and Clamp configurations and positioning. All dimensions are in mm. 37

Figure 3.5 Experimental C-scan showing the delamination pattern obtained after the impact test (left), load-displacement curve (middle) and internal energy curve (right) (taken from González et al. [8]). 38
Figure 3.6 Through-thickness modelling strategy. 39
Figure 3.7 Abaqus finite element assembly. 39
Figure 3.8 Finite element mesh adopted in the Abaqus model. 40
Figure 3.9 Nonlinear in-plane shear hardening curve implemented in the Abaqus Ply Fabric material model. 42
Figure 3.10 Reconstruction of the bi-linear compressive softening law proposed by González et al. 46
Figure 3.11 Comparison between the reference bi-linear softening law and the exponential softening law implemented in the present Abaqus model. 47
Figure 3.12 Laminate through-thickness definition 54
Figure 4.1 Comparison of the elastic force–displacement response obtained from the experimental test, the analytical reference model and the numerical models. 62
Figure 4.2 Detailed comparison of the initial contact stage between the experimental response, the analytical reference solution and the numerical models. 63
Figure 4.3 Complete force–displacement response comparing the Layer-wise Model with Cohesive Interfaces and the Adaptive ERR–Cohesive Large-Element Model after the implementation of adaptive delamination. 64
Figure 4.4 Comparison of the complete force–displacement response obtained from the experimental test, the analytical reference model and the Layer-wise Model with Cohesive Interfaces. 65
Figure 4.5 Detailed comparison of the initial loading stage of the force–displacement response. 66
Figure 4.6 Comparison of the internal energy evolution predicted by the Layer-wise Model with Cohesive Interfaces and the analytical reference model. 68
Figure 4.7 Predicted intralaminar damage at the end of the impact simulation: fibre damage in the outer 0° ply 69
Figure 4.8 Predicted intralaminar damage at the end of the impact simulation: fibre damage in the outer 45° ply 69

Figure 4.9 Predicted intralaminar damage at the end of the impact simulation: shear damage 70
Figure 4.10 Comparison of the projected delaminated area predicted by the Layer-wise Model with Cohesive Interfaces and the analytical reference model. 72
Figure 4.11 Global load–displacement response of the Adaptive ERR–Cohesive Large-Element Model compared with the experimental results and the validated reference model proposed by González et al. [8]. 74
Figure 4.12 Internal energy evolution of the Adaptive ERR–Cohesive Large-Element Model compared with the validated reference model proposed by González et al. [8]. 75
Figure 4.13 Influence of the hourglass stiffness coefficient on the predicted delamination morphology: (a) HG = 0.01, (b) HG = 0.1 and (c) HG = 1.5. 76
Figure 4.14 Projected delamination area predicted using four different enriched interface configurations. 79
Figure 4.15 Comparison of the projected delamination area predicted by the Adaptive ERR–Cohesive Large-Element Model using different enriched interface configurations and the validated reference model proposed by González et al. [8]. 80

LIST OF TABLES

Table 2.1 Computational cost comparison between different delamination modelling strategies (adapted from Daniel [16]). 29
Table 2.2 Comparison of the main numerical approaches for delamination modelling. 31
Table 3.1 Specimen Dimensions 34
Table 3.2 Material properties of the CFRP laminate used in the experimental programme and numerical simulations. 36
Table 3.3 Mesh Size data 39
Table 3.4 Comparison between the constitutive modelling strategies adopted by González et al. [8] and the present work. 41
Table 3.5 Damage initiation parameters adopted for the Ply Fabric constitutive model. 43
Table 3.6 Damage propagation parameters adopted for the Ply Fabric constitutive model. 44
Table 3.7 Parameters employed for the reconstruction of the reference bi-linear compressive softening law 45
Table 3.8 Fabric failure parameters adopted for the Ply Fabric constitutive model. 48
Table 3.9 Cohesive Interface properties adopted for the Ply Fabric constitutive model. 49
Table 3.10 Main include files employed in the LS-DYNA model. 53
Table 3.11 Adaptive delamination parameters defined in the MAT_ADAPT_LAMINATE material card. 56
Table 3.12 Additional constitutive parameters required by the LS-DYNA user-defined material model. 58
Table 4.1 Required simulation time for each model 84

LIST OF ABBREVIATIONS AND SYMBOLS

Abbreviations

ASTM	American Society for Testing and Materials
BK	Benzeggagh–Kenane
CAI	Compression After Impact
CFRP	Carbon Fibre Reinforced Polymer
CZM	Cohesive Zone Model
DCB	Double Cantilever Beam
DOF	Degrees of Freedom
ENF	End-Notched Flexure
ERR	Energy Release Rate
FE	Finite Element
FEM	Finite Element Method
LEFM	Linear Elastic Fracture Mechanics
LVI	Low-Velocity Impact
MMB	Mixed-Mode Bending
VCCT	Virtual Crack Closure Technique

Symbols

E_1	Longitudinal Young's modulus
E_2	Transverse Young's modulus
G_{12}	In-plane shear modulus
V_{12}	Major Poisson's ratio
ρ	Major Poisson's ratio
X_1^+	Longitudinal tensile strength
X_1^-	Longitudinal compressive strength
X_2^+	Transverse tensile strength
X_2^-	Transverse compressive strength
X_6	In-plane shear strength

T	Interlaminar tensile strength
S	Interlaminar shear strength
GI_C	Mode I critical fracture toughness
GII_C	Mode II critical fracture toughness
$GIII_C$	Mode III critical fracture toughness
G_1^+	Longitudinal tensile fracture toughness
G_1^-	Longitudinal compressive fracture toughness
G_2^+	Transverse tensile fracture toughness
G_2^-	Transverse compressive fracture toughness
G_6	Shear fracture toughness
G	Total Energy Release Rate
GI	Mode I Energy Release Rate
GII	Mode II Energy Release Rate
$GIII$	Mode III Energy Release Rate
G_C	Critical Energy Release Rate
A	Crack area
d	Damage variable
δ	Relative displacement jump
δ_0	Displacement at damage initiation
δ_C	Critical separation displacement
t_I	Mode I cohesive traction
t_{II}	Mode II cohesive traction
t_{III}	Mode III cohesive traction
t_{eq}	Equivalent traction
$k\alpha$	Penalty stiffness
Δx	Relative sliding displacement
Δy	Relative opening displacement
ΔA	Crack extension area
σ_{12}	In-plane shear stress
$\bar{\sigma}_{12}$	Effective shear stress
εp_{12}	Equivalent plastic shear strain
ε_o	Damage initiation strain

THIS PAGE WAS INTENTIONALLY LEFT BLANK

1. INTRODUCTION

Fibre-reinforced polymer (FRP) composites have become an important class of structural materials in modern engineering applications. Their high specific stiffness and strength, combined with corrosion resistance and design flexibility, have led to their widespread use in sectors such as aerospace, automotive and renewable energy systems [1], [2]. As a result, composite structures are increasingly replacing traditional metallic components in weight-critical applications.

Despite these advantages, laminated composites exhibit complex damage mechanisms that differ significantly from those found in isotropic materials. Among these mechanisms, delamination, defined as the separation between adjacent plies of the laminate, represents one of the most critical failure modes in composite structures. This damage mechanism may lead to a significant reduction in structural stiffness and load-carrying capability, and it can propagate internally within the laminate without obvious surface indications [3], [4].

Due to its importance, the prediction of delamination has been widely investigated in the field of computational structural mechanics. Finite element modelling has become the primary tool for analysing these damage processes. Over the past decades, several numerical techniques have been developed to simulate delamination initiation and propagation. Among these approaches, Cohesive Zone Modelling (CZM) has gained widespread acceptance because it enables crack growth to be represented through traction–separation relationships defined at the interfaces between adjacent plies [5]. In parallel, fracture-mechanics-based approaches, such as the Virtual Crack Closure Technique (VCCT), have also been successfully applied to predict delamination propagation by evaluating the energy release rates at the crack tip [6].

Although these modelling approaches provide accurate predictions of delamination behaviour, they typically require very refined meshes in the vicinity of the fracture process zone. This requirement can considerably increase the computational cost of the simulations, particularly when large structural models are analysed [7].

Finite element models integrating shell elements with cohesive interface formulations have proven effective in reproducing complex damage mechanisms in composite laminates. This modelling strategy has been successfully applied to simulate low-velocity impact events and Compression-After-Impact (CAI) behaviour, enabling the prediction of both intralaminar and interlaminar damage mechanisms [8], [9]. However, conventional cohesive modelling techniques still require relatively fine discretisation, which also limits their efficiency when applied to large composite structures.

To address these limitations, recent research has focused on the development of modelling strategies capable of predicting delamination propagation while reducing mesh dependency and computational effort. An example is the energy-release-rate-based cohesive formulation proposed in [10], which permits the simulation of delamination propagation using relatively large finite elements. This approach integrates concepts from fracture mechanics and cohesive modelling to improve computational efficiency.

More recently, this approach has been further extended to account for arbitrarily shaped delamination fronts using large and potentially distorted elements, which significantly improves its applicability to complex structural configurations [11].

Although these developments represent a significant step towards efficient delamination modelling, further work is required to evaluate their performance in real structural scenarios. In particular, their application to large-scale composite structures still requires additional validation. For this reason, the present thesis focuses on the application and validation of this interlaminar damage modelling approach in large-scale structural models, with the aim of assessing its predictive capability and computational efficiency.

1.1. Motivation

As discussed in the Introduction, the accurate prediction of delamination is essential for the structural analysis and design of composite structures. While several numerical techniques have been developed to model this damage mechanism, their application to large structural models remains challenging.

Many existing approaches require a refined mesh discretisation to accurately capture the fracture process zone associated with delamination propagation. Although this level of discretisation is feasible for small-scale coupon tests and simplified structural models, its application to large composite structures often results in a substantial increase in computational cost.

Recent developments in delamination modelling have therefore focused on improving the computational efficiency of numerical simulations. In this context, the energy-release-rate-based cohesive formulation proposed in [10] represents an important step towards reducing mesh dependency while maintaining predictive accuracy. Furthermore, the extension of this approach to arbitrarily shaped delamination fronts broadens its applicability to more complex structural configurations [11].

Despite these promising developments, further validation is still required to assess the performance of these modelling approaches when applied to large-scale structural models. In particular, it is important to determine whether the use of larger finite elements can accurately predict delamination propagation while preserving computational efficiency.

Therefore, the motivation of this thesis is to investigate the applicability of the proposed interlaminar damage modelling strategy in large composite structures and to evaluate its performance in terms of accuracy and computational efficiency.

1.2. Objectives

Based on the state of the problem discussed in the previous sections and the modelling framework illustrated in Figure 1.1, the main objective of this thesis is to apply and evaluate an efficient interlaminar damage modelling strategy for the simulation of delamination propagation in large-scale composite structures.

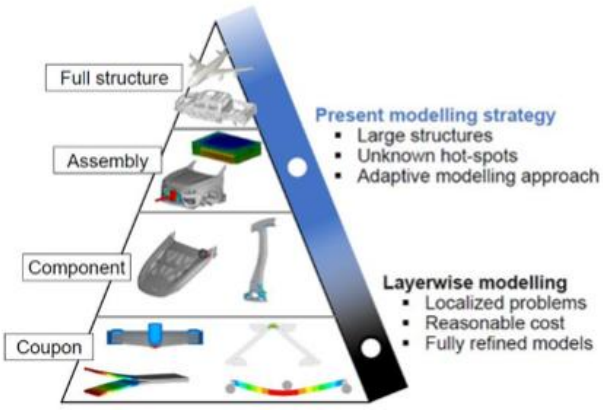


Figure 1.1 Framework for multiscale modelling of delamination in composite structures (after Daniel [16])

More specifically, the work aims to assess the applicability, predictive capability, and computational efficiency of a modelling strategy designed to represent interlaminar failure while remaining suitable for structural-scale finite element analyses.

In order to achieve these specific objectives, the following tasks are addressed:

- Implement the interlaminar damage modelling approach proposed in [10] and [11] within a finite element framework suitable for large-scale structural models.
- Reproduce the finite element modelling strategy for impact simulations in composite laminates described in [8].
- Apply the modelling approach to representative composite structural configurations in order to analyse the initiation and propagation of delamination.
- Compare the obtained results with refined reference models in order to evaluate the accuracy of the proposed modelling strategy.
- Assess the advantages and limitations of the method when applied to large structural models.

Through these objectives, the present work aims to evaluate the potential of the proposed modelling strategy as an efficient tool for the simulation of interlaminar damage in engineering composite structures.

1.3. Structure of the dissertation

This dissertation is organised into five chapters that progressively introduce the research problem, present the adopted methodology, validate the proposed numerical approaches, and discuss the main findings.

Chapter 1 introduces the research topic by presenting the background of interlaminar damage modelling in composite structures, the motivation for the study, the research objectives, and the overall organisation of the dissertation.

Chapter 2 reviews the state of the art on numerical delamination modelling. It begins with fracture mechanics approaches based on the Energy Release Rate (ERR), followed by Cohesive Zone Models (CZM), and concludes with recent hybrid ERR–cohesive formulations developed to improve computational efficiency for large-scale composite structures.

Chapter 3 describes the numerical methodology adopted throughout this work. It first presents the experimental reference programme and then details the development of the two finite element models considered in this study: a conventional layer-wise model with cohesive interfaces implemented in Abaqus and an adaptive ERR–cohesive large-element model implemented in LS-DYNA.

Chapter 4 presents the validation and comparison of both numerical approaches. The predicted force–displacement response, energy evolution and delamination patterns are compared with the experimental observations and the reference numerical model. The computational performance, strengths and limitations of each modelling strategy are also discussed.

Finally, Chapter 5 summarises the principal conclusions of the research, evaluates the achievement of the proposed objectives, discusses the current limitations of the developed models, and outlines recommendations for future work on adaptive interlaminar damage modelling.

THIS PAGE WAS INTENTIONALLY LEFT BLANK

2. LITERATURE REVIEW

Delamination is one of the most critical failure mechanisms in laminated composite structures, as it can significantly reduce the residual strength and stiffness of the laminate while remaining difficult to detect. Consequently, considerable research efforts have been devoted to the development of numerical techniques capable of accurately predicting both the initiation and propagation of interlaminar cracks. This literature review focuses on the numerical approaches most relevant to the methodology adopted in this thesis, highlighting their underlying principles, advantages, limitations, and suitability for the analysis of large composite structures.

Early numerical studies of delamination propagation were primarily based on fracture mechanics concepts, in which crack growth is governed by the Energy Release Rate (ERR). According to this framework, delamination propagates when the energy released by the structure as the crack advances reaches the critical fracture toughness of the material. Numerical implementations of this approach, such as the Virtual Crack Closure Technique (VCCT), have been widely used to evaluate the ERR within finite element models and to simulate delamination propagation. Although these fracture-mechanics-based approaches provide accurate predictions of crack propagation, their application to large structural models is often limited by modelling assumptions and computational requirements.

With the increasing use of the finite element method and the availability of greater computational resources, Cohesive Zone Models (CZM) emerged as an alternative and widely adopted approach for modelling delamination. These models represent the interface behaviour through traction–separation laws that describe the progressive degradation of the material ahead of the crack tip, thereby enabling both damage initiation and propagation to be captured within the numerical model.

Although both ERR-based approaches and Cohesive Zone Models (CZM) have proven effective in many applications, their use in large composite structures can be computationally demanding or limited by modelling assumptions. To address these challenges, recent research

has focused on hybrid modelling strategies that combine the advantages of both approaches. Among these developments, hybrid formulations combining Energy Release Rate (ERR) criteria with cohesive formulations have emerged as a promising solution for balancing predictive capability and computational efficiency. These approaches constitute the basis of the modelling strategy investigated in this thesis and provide the framework for the numerical models presented in the following chapters.

2.1. Energy Release Rate Methods for Delamination Modelling

Delamination propagation in laminated composite structures has traditionally been analysed within the framework of Linear Elastic Fracture Mechanics (LEFM). In this approach, crack growth is governed by the concept of Energy Release Rate (ERR), which represents the rate at which elastic strain energy is released as a crack propagates through a material. Within this theoretical framework, crack propagation occurs when the available energy release rate reaches the critical energy release rate (fracture toughness) of the material interface.

Mathematically, the energy release rate can be expressed as the derivative of the total potential energy of the system with respect to the crack area:

$$G = \frac{d\Pi}{dA} \tag{2.1}$$

Equation (2.1) indicates that crack propagation is governed by the balance between the elastic energy released by the structure and the energy required to create new fracture surfaces, where Π is the total potential energy and A is the crack surface area. This formulation originates from the Griffith energy balance criterion, which states that crack growth occurs when the energy released by the structure as the crack advances becomes equal to or greater than the critical energy required to generate new fracture surfaces. For delamination problems, this critical quantity is generally associated with the fracture toughness of the interface [12].

In laminated composite materials, delamination occurs at the interface between adjacent plies and may develop under different loading conditions. Three fundamental fracture modes

are typically considered: mode I (opening mode), mode II (sliding mode) and mode III (tearing mode), see Figure 2.1. In practice, delamination growth usually occurs under mixed-mode conditions, where different fracture modes act simultaneously. Consequently, the total energy release rate is commonly decomposed into modal components:

$$G = G_I + G_{II} + G_{III} \tag{2.2}$$

where G_I, G_{II}, and G_{III} correspond to the energy release rates associated with opening, in-plane shear and tearing modes respectively.

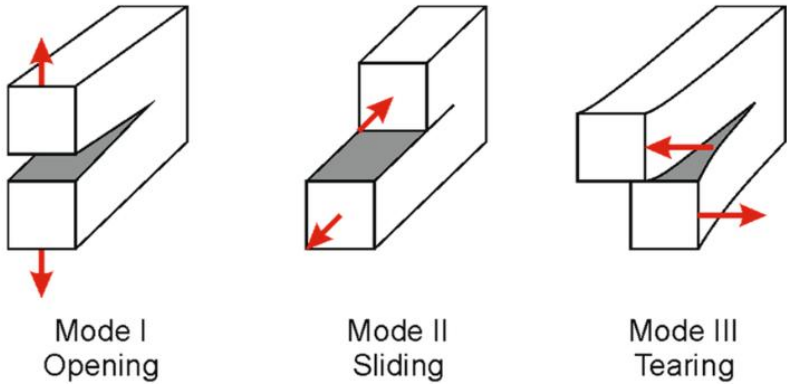


Figure 2.1 Schematic representation of the three fundamental delamination fracture modes in laminated composites: Mode I (opening), Mode II (sliding) and Mode III (tearing). Adapted from Hull and Clyne [2].

To determine whether crack propagation occurs under mixed-mode conditions, the calculated energy release rate must be compared with a mixed-mode fracture criterion. Several criteria have been proposed in the literature, among which the Benzeggagh–Kenane criterion is one of the most widely used for composite laminates. This empirical law relates the critical fracture toughness to the proportion of shear and opening modes and has been extensively validated experimentally [13]. The B–K criterion is expressed as:

$$G_c = G_{Ic} + (G_{IIc} - G_{Ic}) * \left(\frac{G_{II} + G_{III}}{G_I + G_{II} + G_{III}}\right)^n \tag{2.3}$$

where Gc is the mixed-mode critical energy release rate, G_{Ic} and G_{IIc} are the critical energy release rates under pure Mode I and Mode II loading, respectively, G_I, G_{II}, and G_{III} are the energy release rate components associated with opening, sliding, and tearing modes, and η is

the material-dependent Benzeggagh–Kenane exponent, determined experimentally to characterize the influence of mode mixity on the fracture toughness.

The Energy Release Rate therefore provides the fundamental parameter governing crack propagation in fracture-mechanics-based approaches. Numerical methods such as the Virtual Crack Closure Technique employ this concept to evaluate the ERR directly from finite element results, as described in the following section.

2.1.1. Virtual Crack Closure Technique

The Virtual Crack Closure Technique (VCCT), originally proposed by Rybicki and Kanninen [14], is one of the most widely adopted numerical methods for evaluating the Energy Release Rate (ERR) within finite element analyses. The method is based on the assumption of self-similar crack growth, whereby the energy required to close a crack over a small increment is equal to the energy released when the crack extends by the same increment. This concept enables the ERR to be computed directly from nodal forces and relative displacements around the crack tip.

Originally introduced in fracture mechanics for finite element analyses, the VCCT evaluates the energy release rate using nodal forces and relative displacements around the crack tip [14]. The crack-tip configuration used for the evaluation of the energy release rate in the VCCT formulation is illustrated in Figure 2.2. For instance, in the case of fracture Mode I, the energy release rate can be approximated as:

$$G_I = \frac{1}{2\,\delta A} F_y \Delta_{A+\delta A} \tag{2.4}$$

where Fy represents the nodal force normal to the interface at the crack tip, $\Delta_{A+\delta A}$ is the relative opening displacement between the nodes immediately behind the crack tip, and δA is the crack extension length. Although the VCCT formulation is conceptually straightforward, its practical implementation can become computationally demanding. The classical crack closure procedure, see Figure 2.2, requires two analyses at each load increment in order to obtain the forces and relative displacements needed to evaluate the energy release rate. This requirement becomes particularly inconvenient in three-dimensional problems, where

multiple potential crack propagation directions must be evaluated along the delamination front.

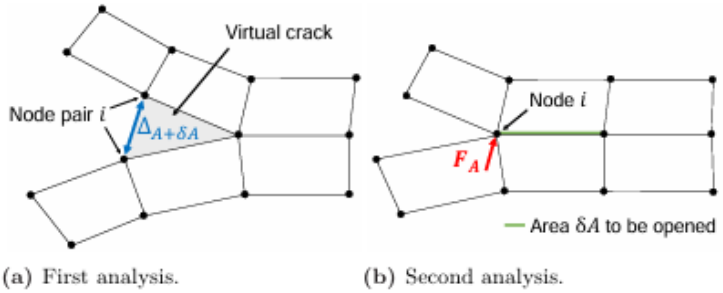


Figure 2.2 Schematic representation of the Crack Closure Technique used to compute the energy release rate [16].

Nonetheless, in the VCCT, the quantities required to evaluate the energy release rate can be obtained from a single finite element analysis, avoiding the need to perform two separate analyses for each load increment. Under the assumption of self-similar crack growth, the nodal force *FA* acting at node *i* is assumed to be equal to the force acting at node *i+1* after the virtual crack extension. The relative displacement measured at the node pair immediately behind the crack front is used to approximate the crack opening of the virtual crack extension, while the nodal forces acting at the crack tip are extracted from the same numerical solution. This allows the modal components of the energy release rate to be computed directly from the nodal forces and relative displacements obtained in the finite element model [6].

Therefore, under the latter assumptions, the modal components of the energy release rate can be expressed as:

$$G_I = \frac{1}{2\,\delta A^i}\, F_I^i \left\langle \Delta_{\mathbf{I}}^{\mathrm{i}-1} \right\rangle \mathrm{c} \tag{2.5}$$

$$G_{II} = \frac{1}{2\,\delta A^i}\, F_{II}^i \left\langle \Delta_{\boldsymbol{II}}^{i-1} \right\rangle c \tag{2.6}$$

where F_I^i and F_{II}^i correspond to the nodal forces associated with the opening and sliding modes at the crack tip node *i*, $\Delta_{\boldsymbol{I}}^{i-1}$ and $\Delta_{\boldsymbol{II}}^{i-1}$ denote the relative displacements measured at the node pair located behind the crack front, and *δAi* represents the crack extension area

associated with the interface elements ahead of the crack tip. The factor c is a correction coefficient introduced to account for differences in element lengths across the crack front.

The total energy release rate is then obtained by combining the modal contributions, as follows:

$$G = G_I + G_{II} \tag{2.7}$$

The crack-tip configuration used to evaluate these quantities is illustrated in Figure 2.3. In this configuration, the nodal forces are extracted at the crack front while the relative displacements are measured at the node pair immediately behind it. The area corresponding to the next crack increment is determined from the interface elements located ahead of the crack tip. When the propagation condition $G \geq G_c$ is satisfied, the crack advances by releasing the constraint that keeps the corresponding node pair tied along the interface, allowing the delamination front to propagate through the laminate [6].

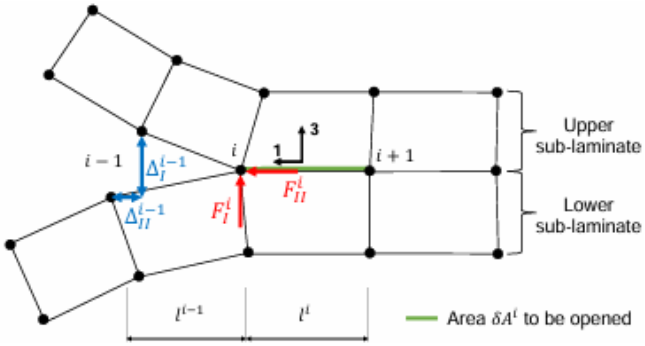


Figure 2.3 Schematic representation of the crack-tip configuration in the VCCT method [16].

The Virtual Crack Closure Technique has been widely applied to simulate delamination propagation in experimental configurations where the crack advances along a predefined path. Typical examples include standard fracture tests such as the Double Cantilever Beam (DCB), End-Notched Flexure (ENF), and Mixed-Mode Bending (MMB) tests, in which the finite element mesh can be aligned with the expected crack growth direction. Under these conditions, the evaluation of the crack opening displacement behind the crack tip and the corresponding crack extension area becomes relatively straightforward.

More complex situations arise when the delamination front is not aligned with the finite element mesh or when distorted elements are present in the model. In such cases, the direct application of the standard VCCT formulation becomes less straightforward and additional numerical procedures are required to accurately evaluate the energy release rate.

To address this issue, several algorithms enabling the modelling of delamination fronts with arbitrary geometries have been proposed in the literature. In particular, Xie et al. [17,18] developed formulations for computing the strain energy release rate of moving crack fronts with arbitrary shapes in regular meshes. These methods were subsequently extended by Liu et al. [19,20], who proposed improved techniques for representing irregular crack front geometries during propagation. More recently, Marjanović et al. [21] further developed these approaches to enable their application to meshes containing distorted elements and more complex laminate configurations.

2.1.2. Efficiency of VCCT for Large Structural Models

One of the principal advantages of VCCT is that its propagation criterion is independent of the size of the fracture process zone (FPZ). Because the method is based on energy balance rather than on a local damage law, it does not require the fracture process zone to be explicitly resolved by the finite element mesh [5].

This characteristic allows VCCT to be used with relatively large finite elements, which significantly reduces computational cost. Consequently, the number of interface elements and the overall number of degrees of freedom can be significantly reduced compared with cohesive zone formulations. Several studies have demonstrated that accurate delamination propagation predictions can be obtained using element sizes up to approximately 5 mm [22].

For this reason, VCCT represents a promising approach for the efficient modelling of delamination growth in large composite structures, where cohesive zone models may require extremely fine meshes to capture the fracture process zone.

Recent studies have explored the use of VCCT in more complex scenarios, including the modelling of partially reinforced Double Cantilever Beam [23] specimens and low-velocity impact [24] events in composite laminates. These studies confirm that VCCT remains computationally efficient even when applied to complex propagation problems.

2.1.3. Limitations of VCCT

Despite its advantages, several limitations have been identified when using VCCT to model delamination propagation.

A major limitation arises from the fact that crack growth in classical VCCT implementations is discrete and directly linked to the element size. Once the propagation criterion $G \geq Gc$ is satisfied, the crack advances to the next element interface. Consequently, the crack increment is proportional to the element size, which may lead to a poor discretisation of the delamination front during propagation. This discrete propagation behaviour can introduce numerical artefacts. In particular, irregular crack front geometries may produce large nodal forces at corner nodes, leading to local overestimations of the energy release rate. As a result, the predicted crack propagation speed may be artificially increased [6,22,23].

Another limitation is that VCCT does not explicitly represent progressive crack growth mechanisms occurring within the fracture process zone. In real composite interfaces, delamination propagation occurs through micro-mechanical damage processes such as matrix cracking, fibre bridging and interface debonding. Since VCCT treats the crack tip as a singular point, these mechanisms are not captured [7,9,24].

2.1.4. Progressive Node Release Methods

To address these limitations, several researchers have proposed modifications to the classical VCCT formulation to improve the stability of crack propagation simulations. In particular, Daniel et al. [10] and Daniel [16] introduced strategies aimed at improving the numerical

behaviour of ERR-based approaches when modelling delamination propagation with large finite elements.

One promising strategy consists of progressively releasing the constraint at the crack front once the propagation criterion is satisfied. Instead of instantaneously releasing the node when $G \geq Gc$, the constraint is gradually relaxed over several increments. As discussed by Daniel [16], this progressive node release enables the fracture energy associated with the newly created crack surface to be dissipated more smoothly, thereby reducing artificial energy concentrations at the crack tip and improving numerical stability.

This approach is particularly advantageous in dynamic simulations, where sudden crack propagation may generate numerical oscillations caused by the abrupt release of strain energy. It therefore represents an effective improvement over the classical VCCT formulation while preserving its computational efficiency.

Other developments have focused on extending VCCT to arbitrary crack front geometries and distorted meshes, broadening its applicability to more complex structural analyses [17–21].

Despite these improvements, VCCT-based methods still require an initial crack to be predefined before crack propagation can be simulated. As highlighted by Krueger [6], this remains one of the principal limitations of fracture-mechanics-based approaches and provided the motivation for the development of Cohesive Zone Models, discussed in the following section.

2.2. Cohesive Zone Models for Delamination

2.2.1. Fundamentals

The constitutive behaviour of the cohesive interface in composite laminates is commonly described through a traction–separation relationship, which defines how the interface tractions evolve as the relative displacement between two adjacent plies increases. In this formulation, the displacement discontinuity across the interface is related to the stresses transmitted between the plies, allowing the progressive degradation of the interface to be represented within the finite element model [7].

In most cohesive formulations, the traction–separation response consists of an initial linear elastic stage, followed by a softening regime that represents the progressive degradation of the interface. One of the most widely adopted representations is the bilinear traction–separation law, which is characterised by three main parameters:

- an initial penalty stiffness, which defines the proportional relationship between the interface traction and the relative separation imposed in the finite element model before damage initiation.
- a maximum interface strength defining the onset of damage
- a fracture energy governing complete separation.

This formulation ensures that the area under the traction–separation curve corresponds to the fracture toughness of the interface, thereby maintaining consistency with classical fracture mechanics principles [12].

Figure 2.4 illustrates the typical traction–separation behaviour used in cohesive interface models. Initially, the interface behaves elastically and the traction increases linearly with the displacement jump. Once the traction reaches its maximum value, damage initiates at the interface and the stiffness progressively degrades until complete separation occurs.

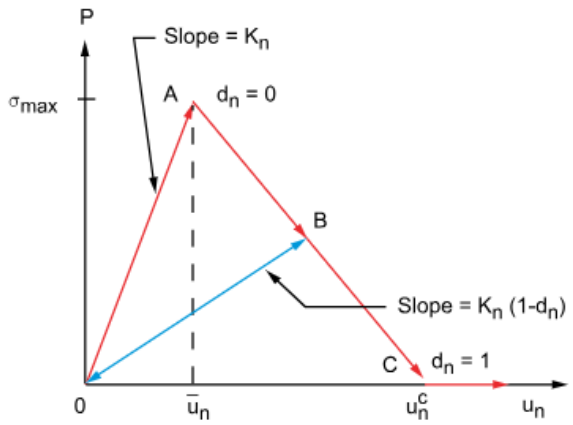


Figure 2.4 Traction–separation law for a cohesive interface element showing elastic behaviour, damage initiation and progressive stiffness degradation until complete separation [25].

The degradation of the interface stiffness is commonly represented through a scalar damage variable d, which evolves from 0 for an undamaged interface to 1 for complete separation. As damage develops, the effective stiffness of the interface is progressively reduced, allowing the model to reproduce the fracture process zone associated with delamination propagation.

For a three-dimensional interface, the constitutive behaviour must account for the three fracture modes involved in delamination:

- opening (mode I);
- sliding (mode II);
- tearing (mode III).

These modes are associated with the displacement jumps across the interface and their corresponding tractions. A commonly used representation of the cohesive constitutive law is given by

$$t_I = k_I\,(1-d)\,\langle \Delta_I \rangle \tag{2.8}$$

$$t_{II} = k_{II}\,(1-d)\,\Delta_{II} \tag{2.9}$$

$$t_{III} = k_{III}\,(1-d)\,\Delta_{III} \tag{2.10}$$

where $t\alpha$ represents the traction in mode α, Δ_α denotes the displacement jump across the interface, k_α corresponds to the interface stiffness and d is the scalar damage variable describing the degradation of the interface stiffness [7].

The behaviour of the cohesive interface for pure loading modes is illustrated in Figure 2.5, where the traction–separation relationships for opening and shear loading are presented. These constitutive laws form the basis for many numerical implementations of cohesive zone models used to simulate delamination growth in laminated composite structures.

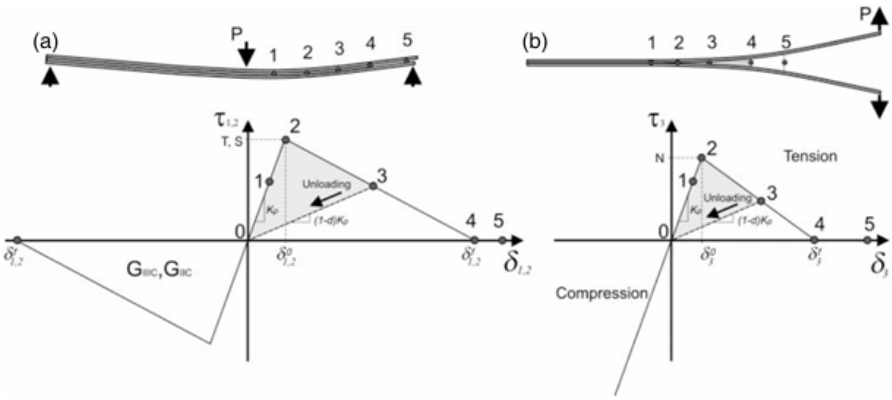


Figure 2.5 Traction–separation relationships for pure loading modes in cohesive interface models: (a) shear loading (mode II/III) and (b) opening loading (mode I), taken from Camanho et al. [7].

2.2.2. Damage Initiation Criteria

Within the cohesive zone modelling framework, the onset of interfacial damage is defined through a damage initiation criterion, which determines when the interface begins to lose stiffness. As discussed in Section 2.2.1, cohesive formulations typically assume an initial linear elastic traction–separation response governed by an interface stiffness parameter. Once the traction acting across the interface reaches a critical value associated with the interlaminar strength, the interface begins to degrade, and the damage variable starts to evolve. This type

of cohesive formulation has been widely used to simulate delamination processes in composite laminates and structural components [7].

In cohesive formulations developed for composite delamination modelling, the constitutive behaviour of the interface is often described using an equivalent traction together with an equivalent displacement jump, which combines the contributions of the normal and shear components of the traction–separation law. This representation allows the cohesive interface behaviour to be expressed in a unified manner under mixed-mode loading conditions, where several fracture modes may act simultaneously along the delamination front [26]. In this framework, the equivalent traction, t_{eq}, is defined as the norm of the traction components acting on the interface:

$$t_{eq} = \sqrt{t_I^2 + t_{II}^2 + t_{III}^2} \tag{2.11}$$

where t_I, t_{II}, and t_{III} denote the traction components associated with opening, sliding and tearing modes, respectively. Damage initiation occurs when the equivalent traction reaches a critical value μ_0, which represents the maximum traction that the interface can sustain before the onset of damage. This interface strength parameter is directly related to the interlaminar strengths of the composite material and marks the beginning of micro-mechanical damage processes occurring within the fracture process zone of the interface.

The cohesive interface behaviour is therefore characterised by three key parameters: the penalty or interface stiffness governing the initial elastic response, the interface strength controlling damage initiation, and the fracture toughness defining the total energy dissipated during crack propagation. In cohesive zone models, the traction–separation response remains linear until the interface strength is reached, after which the interface enters a softening regime associated with the progressive degradation of the cohesive stiffness (see Figure 2.4). As highlighted in studies on cohesive models for composite laminates, the accurate identification of these parameters is essential for predicting both the onset of delamination and its subsequent propagation [23]. Similar conclusions have been reported in studies investigating the interaction between matrix cracking and delamination in composite

laminates, where cohesive formulations were successfully used to simulate complex damage mechanisms [24].

In practical structural applications, delamination rarely occurs under pure opening conditions. Instead, crack propagation generally develops under mixed-mode loading, where normal and shear stresses act simultaneously along the interface. To account for this interaction, cohesive formulations typically incorporate mixed-mode damage initiation criteria that combine the contributions of the different traction components. A commonly used approach is the quadratic interaction criterion, which determines the onset of damage according to:

$$\left(\frac{t_I}{t_I^0}\right)^2 + \left(\frac{t_{II}}{t_{II}^0}\right)^2 + \left(\frac{t_{III}}{t_{III}^0}\right)^2 = 1 \tag{2.12}$$

where t_I, t_{II}, and t_{III} are the traction components associated with Modes I, II, and III, respectively, while t_I^0, t_{II}^0, and t_{III}^0 denote the corresponding interlaminar strengths. Damage initiation occurs when the quadratic interaction function reaches unity, indicating that the interface has reached its strength limit under mixed-mode loading [7,26].

Once the damage initiation condition is satisfied, the cohesive interface enters the damage evolution stage, where the progressive degradation of the interface stiffness governs crack propagation. The formulation of this evolution law, which ensures that the correct amount of fracture energy is dissipated during delamination growth, is discussed in the following section.

2.2.3. Damage Evolution Laws

Once the damage initiation criterion is satisfied, the cohesive interface enters the damage evolution stage, during which the progressive degradation of the interface stiffness governs delamination propagation. In cohesive zone models, this degradation is typically represented by a damage variable, *d*, which evolves from 0 (undamaged interface) to 1 (complete failure). The traction transmitted across the interface is therefore reduced according to the level of damage, allowing the gradual separation of adjacent plies to be captured within the finite element formulation, as described in cohesive formulations for composite laminates [7].

The evolution of damage is usually defined as a function of an equivalent displacement jump λ, which combines the normal and shear components of the interface separation. Initially, the cohesive interface behaves elastically until the displacement reaches λ^0, corresponding to the onset of damage. Beyond this point, stiffness progressively degrades and the transmitted traction decreases until the critical separation displacement λ^c is reached, at which the interface is no longer able to transfer cohesive tractions. This behaviour is commonly represented by a bilinear traction–separation law, illustrated in Figure 2.6, which provides a simple yet effective representation of the fracture process zone in composite interfaces [26].

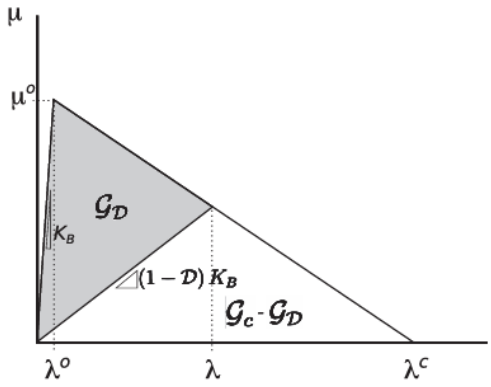


Figure 2.6 Bilinear traction–separation law describing damage initiation and evolution in cohesive zone models (taken from Turon et al. [28]).

The bilinear traction–separation relationship defines the amount of energy dissipated during crack growth. In cohesive formulations, the area under the traction–separation curve corresponds to the fracture energy Gc required to create a new crack surface. Ensuring that the cohesive law dissipates the correct fracture energy is essential for obtaining accurate predictions of delamination propagation in numerical simulations. As shown by Turon et al. [28], an appropriate definition of the cohesive stiffness and strength parameters is necessary to guarantee both numerical stability and correct energy dissipation during crack growth.

In composite laminates, delamination propagation generally occurs under mixed-mode loading conditions, where opening and shear contributions vary along the crack front. To

account for this behaviour, the fracture toughness used in the cohesive formulation is often expressed as a function of the mode mixity. One of the most widely adopted approaches is the Benzeggagh–Kenane (BK) criterion, which relates the mixed-mode fracture toughness to the fracture energies associated with pure mode I and mode II loading [13]. This criterion allows the fracture toughness to increase with the proportion of shear loading, providing a realistic representation of mixed-mode delamination propagation.

The accurate modelling of the damage evolution stage is particularly important because it controls the rate of crack propagation and the amount of energy dissipated during delamination growth. Previous studies have shown that the cohesive parameters governing the softening behaviour strongly influence the predicted structural response. In particular, Turon et al. [28] demonstrated that the definition of cohesive strengths and penalty stiffness values can significantly affect the predicted numerical response, while Sarrado et al. [27] highlighted that inconsistencies in the treatment of mixed-mode energy dissipation may lead to inaccurate predictions of delamination propagation.

Through this formulation, cohesive zone models can represent the progressive degradation of the interface and the associated fracture energy dissipation, providing a physically consistent framework for simulating delamination propagation in composite laminates. However, accurately resolving the fracture process zone often requires relatively fine finite element meshes, which may increase the computational cost when analysing large structural components. This limitation motivates the development of more efficient modelling strategies, which will be discussed in the following sections.

2.2.4. Advantages and Limitations of CZM

Cohesive Zone Models (CZM) are among the most widely used numerical approaches for simulating delamination in composite laminates. Their main advantage is the ability to represent both damage initiation and progressive crack propagation through traction–separation laws, allowing the fracture process zone to be explicitly captured within the finite element formulation. Consequently, cohesive models can reproduce the gradual degradation

of the interface stiffness and the associated dissipation of fracture energy during crack growth [7].

Another important advantage is their capability to represent mixed-mode fracture behaviour. By combining appropriate damage initiation and evolution criteria, such as the Benzeggagh–Kenane criterion, cohesive formulations accurately capture the interaction between opening and shear loading, providing good agreement with experimental observations [13].

As a result, CZM has been successfully applied to numerous structural problems, including low-velocity impact, compression-after-impact (CAI) and fatigue-driven delamination. For example, González et al. [8] demonstrated that cohesive formulations combined with shell finite element models can accurately reproduce both impact damage and the subsequent compression response of composite laminates.

Despite these advantages, CZM presents important limitations when applied to large structural models. Accurate representation of the fracture process zone requires a sufficiently refined mesh along the cohesive interface; otherwise, the traction–separation law may not correctly reproduce the energy dissipation process, leading to mesh-dependent predictions. As shown by Turon et al. [5], the cohesive element size must therefore be carefully selected with respect to the cohesive stiffness and fracture energy to ensure reliable results.

The requirement for fine meshes at every potential delamination interface considerably increases the number of degrees of freedom and, consequently, the computational cost of large-scale simulations. In addition, cohesive elements must be inserted along interfaces where delamination is expected, requiring the potential crack path to be defined a priori, even though damage may ultimately develop only over a limited region.

These limitations have motivated the development of hybrid modelling strategies that combine fracture mechanics concepts with cohesive formulations to improve computational

efficiency while preserving the capability to simulate progressive damage. Recent ERR–cohesive approaches successfully integrate the computational efficiency of energy-based crack propagation methods with the damage representation provided by cohesive models, making them particularly attractive for the analysis of large composite structures [10,11].

2.3. Hybrid ERR–Cohesive Approaches for Delamination Modelling

2.3.1. Motivation for Hybrid Formulations

As discussed in the previous sections, both Energy Release Rate (ERR) methods and Cohesive Zone Models (CZM) present advantages and limitations when applied to the simulation of delamination in composite structures. Fracture mechanics approaches such as the Virtual Crack Closure Technique provide an efficient way to evaluate crack propagation based on energy balance principles. However, these methods require the presence of a predefined crack and do not represent the progressive degradation occurring within the fracture process zone.

In contrast, cohesive zone models allow the simulation of both damage initiation and propagation through traction–separation laws that represent the progressive degradation of the interface stiffness. Despite their physical consistency, cohesive formulations require the fracture process zone to be adequately resolved by the finite element mesh. As a result, cohesive models often demand very fine meshes, which may lead to high computational costs when analysing large composite structures.

To overcome these limitations, hybrid modelling strategies have been proposed in which fracture mechanics concepts are combined with cohesive formulations. These approaches aim to preserve the computational efficiency of ERR-based crack propagation methods while incorporating the progressive damage description provided by cohesive models.

2.3.2. ERR–Cohesive Formulation

An important development in this direction was proposed by Daniel et al. [10], who introduced an adaptive ERR–cohesive framework for the simulation of delamination propagation in composite laminates. Unlike conventional cohesive zone models, where cohesive elements are inserted along every potential delamination interface prior to the analysis, this methodology combines an Energy Release Rate (ERR) propagation criterion with a local cohesive formulation that is activated only where delamination occurs. In this way, the method retains the predictive capabilities of cohesive models while significantly reducing the mesh refinement required by conventional CZM formulations.

The methodology is based on an adaptive modelling strategy in which the laminate is initially represented using a single through-thickness finite element (Figure 2.7). Instead of discretising every ply interface with cohesive elements, only the interfaces where delamination is expected are locally enriched by introducing additional interface nodes. This enrichment creates two independent sub-laminates while preserving the original finite element discretisation, concentrating the computational effort only around the propagating crack.

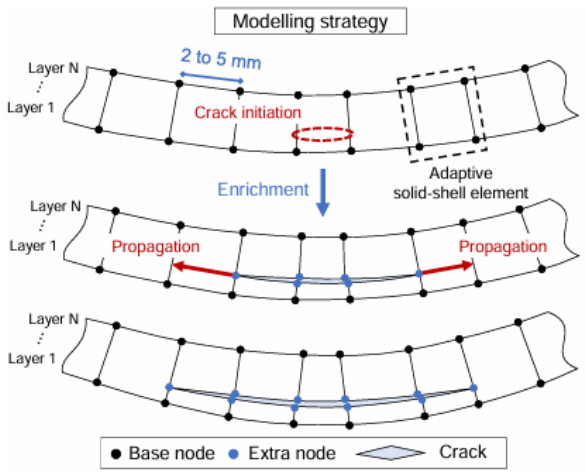


Figure 2.7 Adaptive enrichment strategy proposed by Daniel [16].

Prior to crack propagation, the coincident interface nodes remain kinematically constrained, ensuring displacement compatibility between adjacent sub-laminates. Once the propagation criterion is satisfied, the constraints are progressively released and a cohesive traction–separation law governs the interface response, dissipating the fracture energy associated with crack growth. Unlike conventional cohesive zone models, the cohesive response is activated only around the crack front rather than along the entire interface, avoiding the artificial compliance introduced by pre-inserted cohesive elements [10].

Crack propagation is controlled by the Energy Release Rate (ERR), which is evaluated at every propagation step using the Virtual Crack Closure Technique (VCCT). The mixed-mode energy release rate computed at the crack front is compared with the critical fracture toughness of the interface according to the selected mixed-mode fracture criterion. When the propagation condition is fulfilled, the crack advances to the neighbouring enriched element while the cohesive law ensures that the appropriate amount of fracture energy is dissipated during the propagation process [11] (Figure 2.8). Consequently, the methodology combines the fracture-mechanics basis of VCCT with the progressive energy dissipation provided by cohesive formulations, resulting in a robust and physically consistent representation of delamination growth.

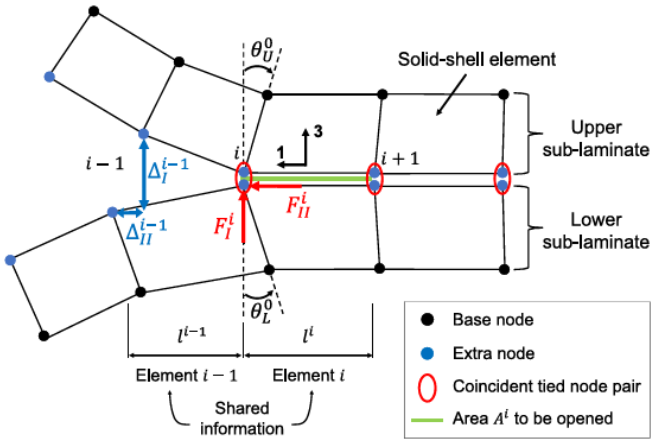


Figure 2.8 Crack-tip configuration employed by the adaptive ERR–cohesive formulation (adapted from Daniel et al. [11]).

Since fracture energy is dissipated according to the area associated with each enriched element rather than through an explicit discretisation of the fracture process zone, the methodology remains accurate with relatively large finite elements. This significantly reduces the number of degrees of freedom and the computational cost, making the approach particularly suitable for large composite structures.

The adaptive ERR–cohesive framework therefore combines the fracture-mechanics basis of VCCT with the progressive damage representation of cohesive formulations, providing an effective balance between predictive capability and computational efficiency. These characteristics make it particularly suitable for the simulation of impact-induced delamination in large composite structures and constitute the basis of the numerical methodology adopted in this dissertation.

2.3.3. Application to Large Structural Models

One of the main motivations behind the development of the ERR–cohesive strategy is to enable the simulation of delamination propagation using relatively large finite elements while preserving numerical accuracy. In conventional cohesive zone models, the element size must be sufficiently small to capture the fracture process zone (FPZ), which typically requires very fine meshes and leads to high computational costs when large structural components are analysed. In contrast, the ERR–cohesive formulation allows the crack propagation process to be controlled by the energy release rate criterion while still representing the interface behaviour through cohesive elements [10,11].

The capability of the method to operate with coarse meshes has been assessed through benchmark simulations involving different element sizes. Figure 2.9 illustrates the evolution of the delamination front predicted using several mesh discretisations. The results obtained with a conventional cohesive zone model implemented in Abaqus using a refined mesh with 0.2 mm interface elements are compared with those obtained using the ERR–cohesive formulation with element sizes of 2 mm and 5 mm. Despite the increase in element size, the predicted crack front remains consistent with the analytical solution and follows the expected circular propagation pattern. These results demonstrate that the ERR–cohesive strategy can

accurately reproduce the global crack propagation behaviour without requiring the very fine discretisation, which is typically needed by conventional cohesive zone models.

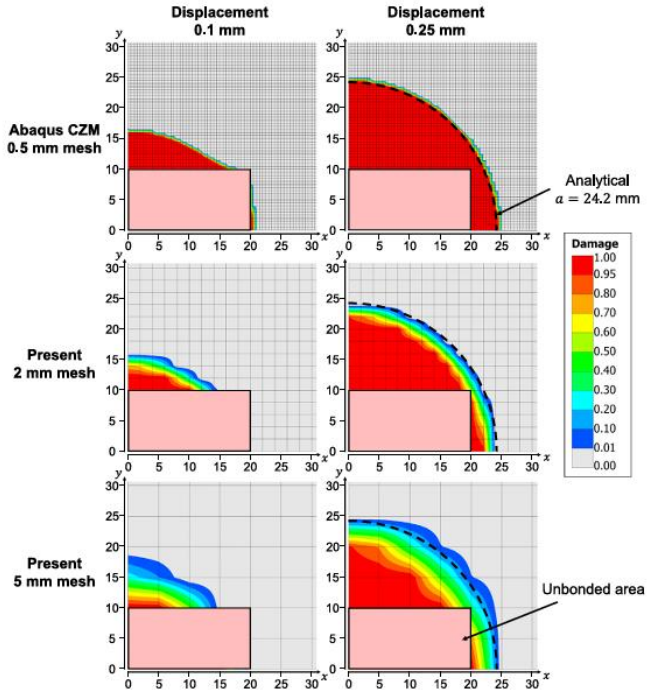


Figure 2.9 Comparison of delamination propagation predicted using conventional cohesive elements and the proposed method with larger finite elements (after Daniel et al. [10]).

These results also demonstrate the robustness of the proposed formulation with respect to element size. Even when element sizes that are one order of magnitude larger than those used in conventional cohesive zone models are employed, the predicted delamination pattern remains stable and physically meaningful. In contrast, conventional cohesive models generally require much finer meshes to accurately capture the fracture process zone, making them more susceptible to mesh dependency when coarse discretisations are used.

The influence of the mesh size on the global structural response can be further analysed by comparing the corresponding force-displacement curves. As shown in Figure 2.10, the response predicted using the proposed approach with element sizes of 2 mm and 5 mm closely follows the analytical solution as well as the results obtained using a conventional cohesive zone model with a refined mesh. Only minor differences are observed in the post-peak regime, which are mainly associated with the discretisation of the crack front. These

results demonstrate that the method can reproduce both the propagation of the delamination front and the overall structural behaviour with good accuracy even when large elements are used.

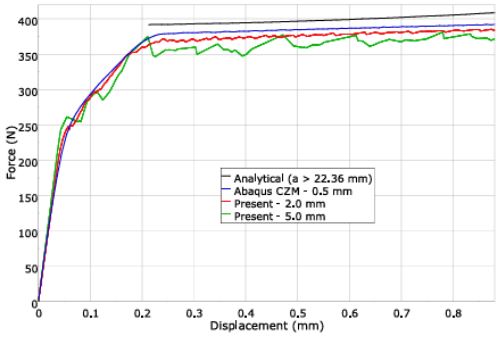


Figure 2.10 Force–displacement response obtained with the proposed large-element approach compared with the analytical solution and a fine-mesh cohesive zone model. Taken from Daniel et al. [10].

From a computational standpoint, this capability represents a significant advantage for the analysis of large composite structures. By enabling the use of coarse meshes without compromising the accuracy of delamination prediction, the ERR–cohesive approach substantially reduces the number of degrees of freedom required in the finite element model. Consequently, the computational cost can be significantly reduced while maintaining reliable predictions of crack initiation and propagation. Compared with conventional cohesive zone modelling, which typically requires element sizes below 1 mm to accurately resolve the fracture process zone, the hybrid formulation enables the use of coarser meshes without compromising the global structural response [10].

Table 2.1 Computational cost comparison between different delamination modelling strategies (adapted from Daniel [16]).

Modelling strategy	Element size	Computational time
Layer-wise cohesive model	0.5 mm	4 h 43 min
Layer-wise cohesive model	2 mm	19 min 46 s
Single-layer model (no delamination)	2 mm	5 min 49 s
Hybrid ERR–Cohesive (2REF)	2 mm	15 min 11 s
Hybrid ERR–Cohesive (1REF)	2 mm	10 min 48 s

A quantitative comparison reported by Daniel [16] further highlights the computational efficiency of the proposed formulation. As summarised in Table 2.1, the hybrid ERR–cohesive approach reduced the computational time from approximately 4 h 43 min required by a conventional 0.5 mm layer-wise cohesive model to around 11–15 min, depending on the enrichment strategy employed. Although the hybrid formulation is slightly more computationally expensive than a single-layer model without delamination, it provides the additional capability of accurately predicting delamination initiation and propagation while remaining suitable for large structural analyses.

2.3.4. Extension to Arbitrary Delamination Fronts

Although the original ERR–cohesive formulation provides an efficient framework for delamination modelling, additional challenges arise when the crack front exhibits complex geometries. In practical structural applications, delamination fronts are rarely straight and may evolve into arbitrarily shaped configurations as the crack propagates.

To address this limitation, further developments were proposed by Daniel et al. [11], who introduced a modelling strategy capable of handling arbitrarily shaped delamination fronts in regular and distorted meshes. This method improves the numerical treatment of the crack front geometry and allows the simulation of delamination propagation in more complex structural configurations.

The proposed formulation enables the robust evaluation of the energy release rate along irregular crack fronts while maintaining the computational efficiency of the hybrid ERR–cohesive approach. As a result, the method extends the applicability of energy-based propagation models to large-scale structural analyses involving complex delamination patterns.

2.4. Critical Comparison of Delamination Modelling Approaches

The numerical approaches reviewed in this chapter present different capabilities depending on the objectives of the analysis. Fracture-mechanics-based methods, such as the Virtual Crack Closure Technique (VCCT), provide an efficient framework for predicting delamination propagation through Energy Release Rate (ERR) calculations. Their main advantage lies in the possibility of using relatively coarse finite element meshes, making them computationally attractive for large structural analyses. However, VCCT requires a predefined crack and cannot directly represent damage initiation or the progressive degradation occurring within the fracture process zone. Table 2.2 presents a comparison between the numerical approaches reviewed in this work for modelling the delamination of FRP.

Table 2.2 Comparison of the main numerical approaches for delamination modelling.

Aspect	VCCT	CZM	Hybrid ERR–Cohesive
Damage initiation	Requires a predefined crack	Predicted through cohesive law	Predicted through local cohesive enrichment
Crack propagation	Energy Release Rate (ERR)	Cohesive damage evolution	Combined ERR and cohesive law
Fracture process zone	Not explicitly represented	Explicitly represented	Locally represented
Mesh sensitivity	Low	High	Low
Computational cost	Low	High	Low–Medium
Large structural models	Suitable	Limited by mesh refinement	Highly suitable
Crack path	Predefined	Potential interfaces predefined	Potential interfaces predefined
Main limitation	Cannot predict damage initiation	High computational cost	More complex implementation

Conversely, Cohesive Zone Models (CZM) provide a unified constitutive framework capable of simulating both damage initiation and propagation through traction–separation laws. This allows the fracture process zone to be explicitly represented and enables accurate predictions

under complex mixed-mode loading conditions. Nevertheless, the need to adequately resolve the fracture process zone generally requires fine mesh discretisation, resulting in a considerable increase in computational cost when analysing large composite structures.

Hybrid ERR–cohesive formulations combine the main strengths of both approaches by introducing cohesive behaviour only where it is required while using Energy Release Rate criteria to govern crack propagation. As a result, they preserve the capability of cohesive models to represent progressive damage while substantially reducing mesh dependency and computational cost. This balance between predictive capability and computational efficiency makes hybrid formulations particularly suitable for the simulation of delamination in large composite structures and provides the basis for the modelling strategy adopted in this dissertation.

Therefore, considering the balance between predictive capability, computational efficiency and applicability to large composite structures, the hybrid ERR–cohesive formulation was selected as the numerical approach investigated in this dissertation.

3. METHODOLOGY

3.1. Experimental Programme

3.1.1. Standard and Reference Study

The experimental configuration reproduced in this work is based on the low-velocity drop-weight impact tests reported by González et al. [8] (see Figure 3.1). These tests were conducted following the ASTM D7136/D7136M standard, which is commonly used to assess the damage resistance of fibre-reinforced polymer matrix composite laminates subjected to out-of-plane impact loading.

In the latter standard test method, a flat rectangular composite plate is impacted by a drop-weight device equipped with a hemispherical striker tip. The resulting damage resistance of the laminate is evaluated in terms of the size, type and location of the damage generated in the specimen.

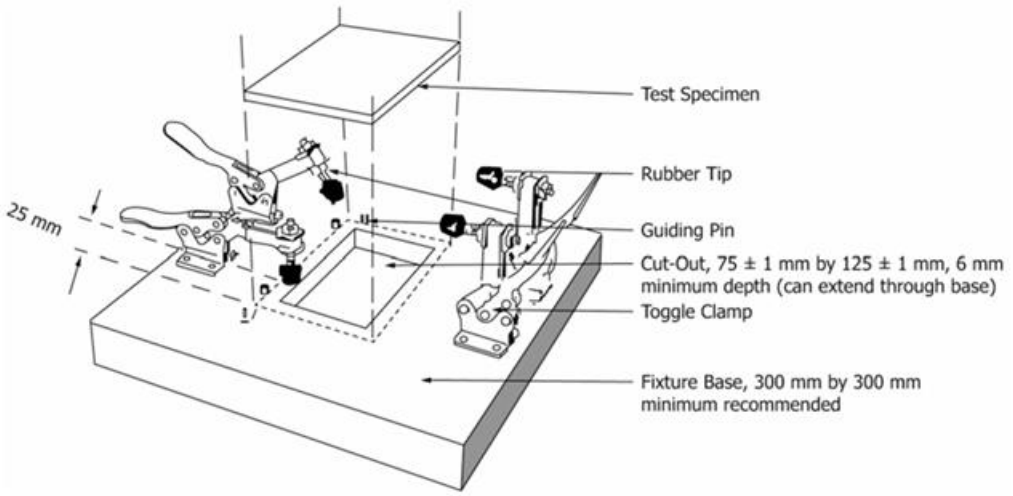


Figure 3.1 Test Configuration Setup

The experimental programme reported by González et al. [8] was adopted as the reference case for the development and validation of the numerical models. Both numerical models

were developed to reproduce the same impact scenario, allowing their predictions of interlaminar damage to be compared under equivalent loading and boundary conditions.

3.1.2. Specimen Geometry and Laminate Configuration

The impact tests were performed on flat rectangular carbon fibre reinforced polymer (CFRP) laminate specimens. The specimen geometry was adopted from the experimental programme reported by González et al. [8], ensuring compatibility with the ASTM D7136/D7136M support fixture and impact configuration.

Each specimen consisted of a twelve-ply laminate with dimensions selected to reproduce the experimental impact configuration. The complete specimen geometry was reproduced identically in both the Abaqus and LS-DYNA numerical models, ensuring that any differences in the predicted damage response were associated with the constitutive modelling approach rather than with geometric variations.

The specimen dimensions are summarised in Table 3.1 and depicted in Figures 3.2 and 3.3, while the laminate stacking sequence and material properties are presented in the following section.

Table 3.1 Specimen Dimensions

Parameter	Value
Length	150 mm
Width	100 mm
Total thickness	4.236 mm
Number of plies	12
Ply thickness	0.353 mm

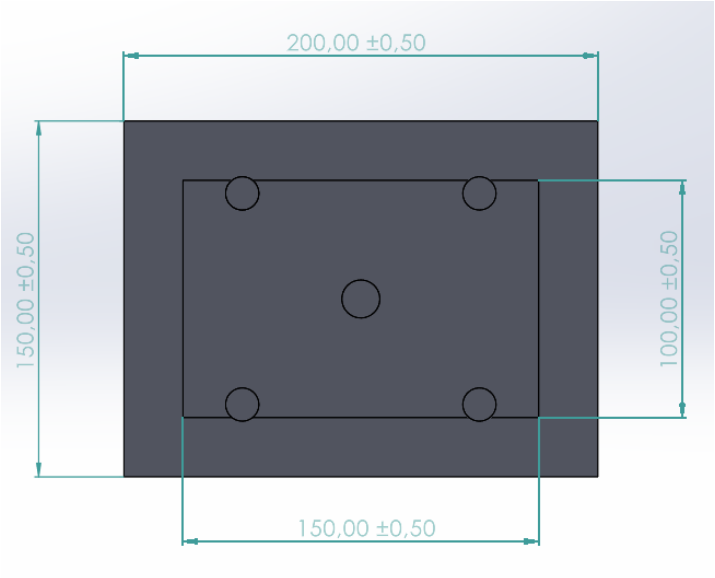


Figure 3.2 Top View Dimensions. All dimensions are in mm.

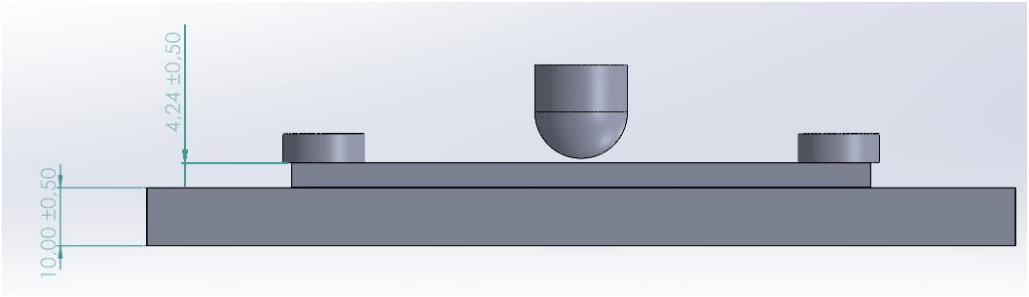


Figure 3.3 Lateral View Dimensions. All dimensions are in mm.

3.1.3. Material and Mechanical Properties

The experimental specimens were manufactured from woven fabric carbon fibre reinforced polymer (CFRP) prepreg laminates. The material system corresponds to that reported by González et al. [8] and was adopted as the reference material for both numerical models developed in this dissertation. The laminate consisted of a symmetric stacking sequence of $[(0,45)_3]s$.

The material characterisation included the elastic properties of the laminate, the strength parameters governing intralaminar failure and the fracture toughness values controlling interlaminar damage propagation. These properties constituted the common material database for both the Abaqus and LS-DYNA models, ensuring that any differences in the

numerical predictions resulted from the constitutive modelling approach rather than from differences in the material definition.

Although identical material properties were employed in both numerical models, their constitutive implementation differs according to the capabilities of each finite element formulation. The corresponding implementations are described in Sections 3.2 and 3.3.
The material properties adopted throughout this work are summarised in Table 3.2.

Table 3.2 Material properties of the CFRP laminate used in the experimental programme and numerical simulations.

Property	**Symbol**	**Value**	**Unit**
Density	ρ	1510	kg/m^3
Longitudinal Young's modulus	E_1	59.54	GPa
Transverse Young's modulus	E_2	54.95	GPa
In-plane shear modulus	G_{12}	5.21	GPa
Major Poisson's ratio	ν_{12}	0.03	-
Longitudinal tensile strength	X_1^+	804.06	MPa
Longitudinal compressive strength	X_1^-	531.29	MPa
Transverse tensile strength	X_2^+	772.77	MPa
Transverse compressive strength	X_2^-	534.11	MPa
In-plane shear strength	X_6	116.9	MPa
Longitudinal tensile fracture toughness	G_1^+	91	N/mm
Longitudinal compressive fracture toughness	G_1^-	10000	N/mm
Transverse tensile fracture toughness	G_2^+	91	N/mm
Transverse compressive fracture toughness	G_2^-	10000	N/mm
Shear fracture toughness	G_6	Not required (NR)	N/mm

3.1.4. Test Setup

The impact tests were performed using the fixture specified in ASTM D7136/D7136M and adopted by González et al. [8]. The specimens were supported on a rigid fixture incorporating a centred rectangular cut-out, allowing the unsupported region of the laminate to deform freely during impact while the specimen edges remained constrained.

The support fixture had overall dimensions of 200 × 150 mm with a centred cut-out measuring 125 × 75 mm. The specimens were secured using four rubber clamping points with a 7 mm radius footprint, preventing rigid body motion while allowing local deformation and damage to develop within the unsupported region of the laminate, Figure 3.4.

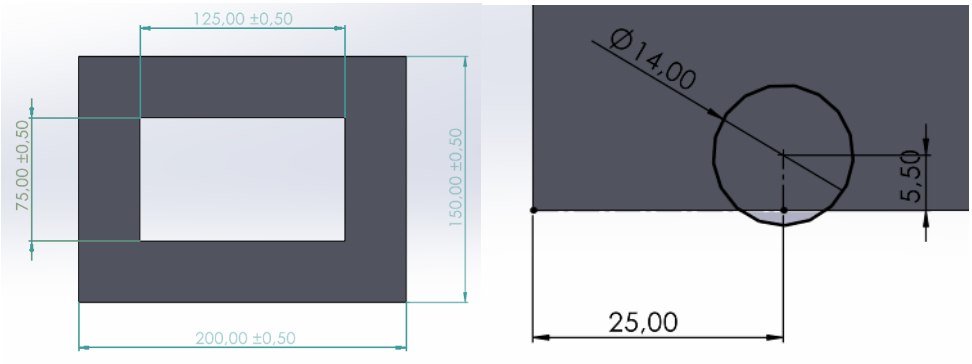


Figure 3.4 Base Opening and Clamp configurations and positioning. All dimensions are in mm.

Impact loading was applied using a 16 mm diameter hemispherical steel impactor positioned above the center of the unsupported area. The impactor had a mass of 5 kg and an initial velocity of 4 m/s, corresponding to an impact energy of approximately 40 J.

3.1.5. Validation Criteria and Experimental Reference Results

Following the impact tests, the damaged specimens were inspected using C-scan ultrasonic testing to characterise the extent of interlaminar delamination. The projected delaminated area at each laminate interface was obtained experimentally, providing the reference dataset for the numerical validation.

Although the experimental programme also reported the global impact response, including the contact force and load–displacement curves, the primary objective of this dissertation is the prediction of impact-induced delamination. Consequently, the numerical models were validated principally by comparing the experimentally measured and numerically predicted delaminated areas.

Figure 3.5 shows the experimental C-scan results, as well as the load-displacement and internal energy relationships reported by González et al. [8].

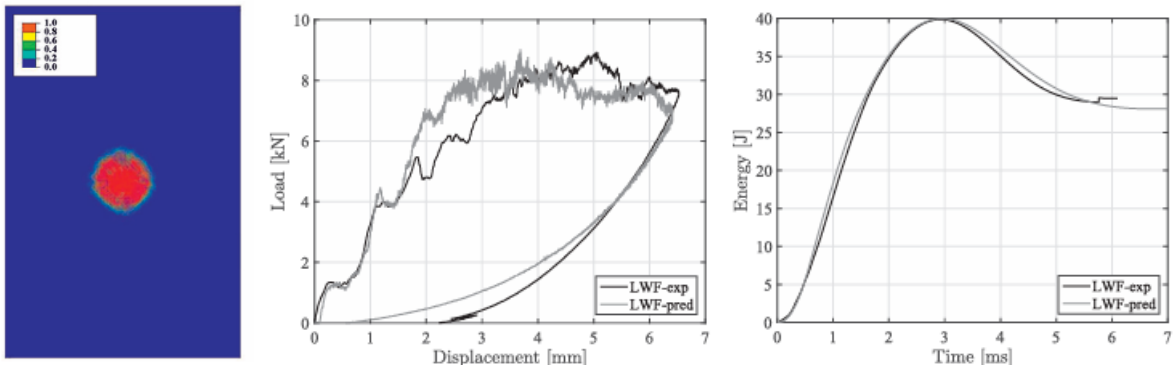


Figure 3.5 Experimental C-scan showing the delamination pattern obtained after the impact test (left), load-displacement curve (middle) and internal energy curve (right) (taken from González et al. [8]).

3.2. Layer-wise Model with Cohesive Interfaces (Abaqus®)

3.2.1. Model Overview

The Abaqus/Explicit finite element software was used to simulate the low-velocity impact tests described in Section 3.1. The laminate was modelled using SC8R continuum shell elements with 8 nodes and reduced integration, while interlaminar delamination was represented by 8-node solid COH3D8 cohesive elements inserted between adjacent plies, resulting in eleven cohesive interfaces through the laminate thickness.

The complete finite element assembly consists of the composite laminate, the hemispherical impactor, the support fixture and the four clamping pads. The laminate was defined as a deformable body, whereas the impactor and supporting components were modelled as

discrete rigid bodies. Figure 3.6 and Figure 3.7 illustrate both the through-thickness discretisation adopted for the laminate and the complete finite element assembly respectively.

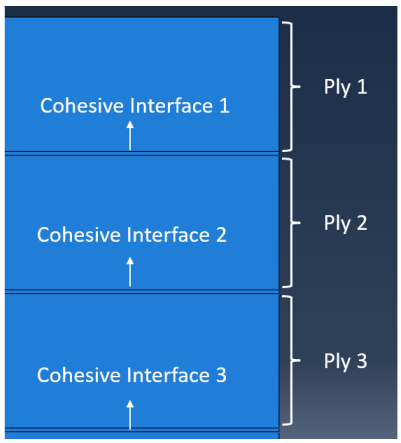


Figure 3.6 Through-thickness modelling strategy.

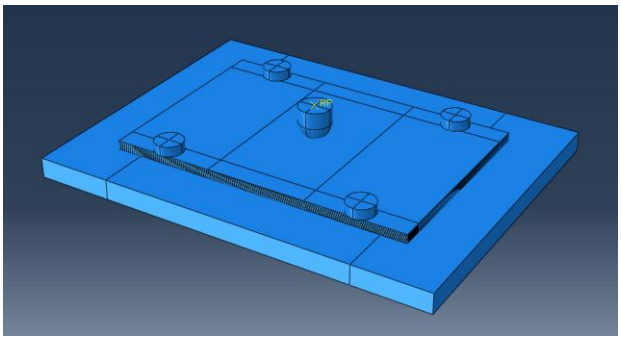


Figure 3.7 Abaqus finite element assembly.

3.2.2. Element and Mesh Discretisation

A locally refined mesh was adopted to accurately capture the high stress gradients generated during impact while maintaining a reasonable computational cost. Following the reference numerical model, a refined region measuring 50 × 80 mm was defined around the impact point and discretised using an element size of 1.5 mm. Outside this region, a progressively coarser mesh was employed to reduce the total number of degrees of freedom.

Table 3.3 Mesh Size data

Region	Element size

Impact zone	1.5 mm
Outer region	Up to 4 mm

A node-to-node correspondence was enforced between the SC8R continuum shell elements and the COH3D8 cohesive elements to ensure displacement compatibility across all laminate interfaces and to enable the correct transfer of interlaminar stresses throughout the simulation.

The final finite element mesh adopted in the Abaqus model is shown in Figure 3.8.

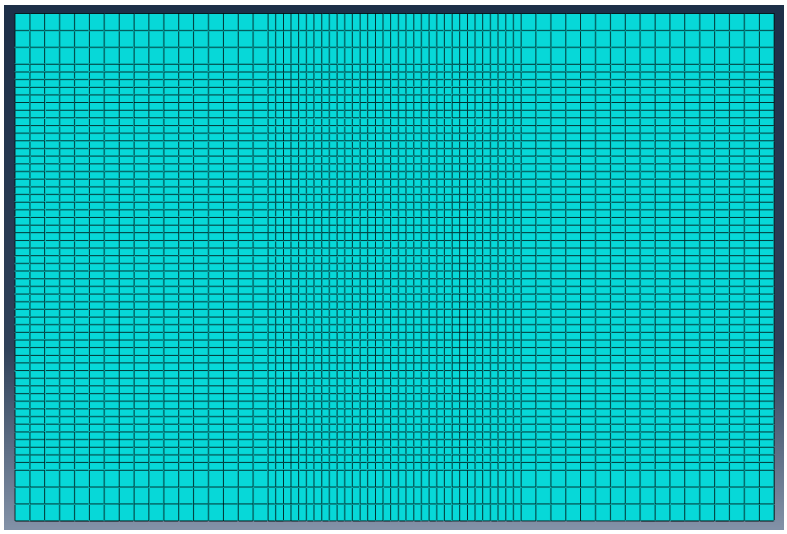


Figure 3.8 Finite element mesh adopted in the Abaqus model.

3.2.3. Laminate Constitutive Modelling

The reference model developed by González et al. [8] employs a user-defined VUMAT, presented by Martín Santos et al. [29], to represent the constitutive behaviour of woven composite laminates. As this user-defined material is not publicly available, an alternative constitutive strategy based exclusively on standard Abaqus material models was adopted.

The woven plies were modelled using the orthotropic Elastic, Type = BILAMINA formulation coupled with the *Ply Fabric* material model. The Bilamina formulation defines the linear elastic response of the woven laminate, whereas the *Ply Fabric* model governs the nonlinear in-plane shear behaviour together with the initiation and evolution of intralaminar damage. Interlaminar delamination was represented independently using COH3D8 cohesive elements inserted between adjacent plies.

The principal differences between the constitutive strategy adopted by González et al. [8] and the implementation developed in the present work are summarised in Table 3.4.

Table 3.4 Comparison between the constitutive modelling strategies adopted by González et al. [8] and the present work.

Original model (González et al. [8])	Present work
User-defined VUMAT	Standard Abaqus material models (ABQ_PLY_FABRIC)
Proprietary constitutive implementation	Bilamina + Ply Fabric
Shell + Cohesive surfaces	SC8R continuum shell elements
Cohesive surfaces	Cohesive elements

The elastic behaviour was defined using Elastic, Type=BILAMINA. The orthotropic elastic properties correspond to those presented in Table 3.2.

Regarding the in-plane shear response, unlike the proprietary VUMAT employed by González et al. [8], the *Abaqus Ply Fabric* formulation requires the nonlinear in-plane shear response to be defined as a tabulated relationship between the equivalent plastic shear stress and the corresponding plastic shear strain.

The reference constitutive model describes this behaviour using the analytical expression proposed by González et al. [8],

$$\sigma_{12} = X_{6P} + \varsigma_E \left(1 - e^{|\varsigma_E^T \varepsilon_{12}^p|}\right) + \varsigma_L \varepsilon_{12}^P \tag{3.1}$$

where X_{6P} represents the shear yield stress, while ς_E, ς_E^T and ς_L are fitting parameters obtained from the experimental ±45° tensile tests.

To ensure consistency with the reference model, the analytical expression was first reconstructed and subsequently sampled to generate the discrete stress–plastic strain data required by the *Abaqus Ply Fabric Hardening* formulation.

During the model development, it was observed that the equivalent plastic shear strain locally exceeded the maximum strain defined by the reconstructed hardening curve. To prevent numerical extrapolation by Abaqus, the hardening law was extended beyond the experimentally characterised range while preserving the asymptotic behaviour of the analytical function. Consequently, the experimentally validated constitutive response remained unchanged, whereas the extended region ensured a smooth and stable material response throughout the impact simulation.

The final hardening curve implemented in the Abaqus model is compared with the original analytical response in Figure 3.9.

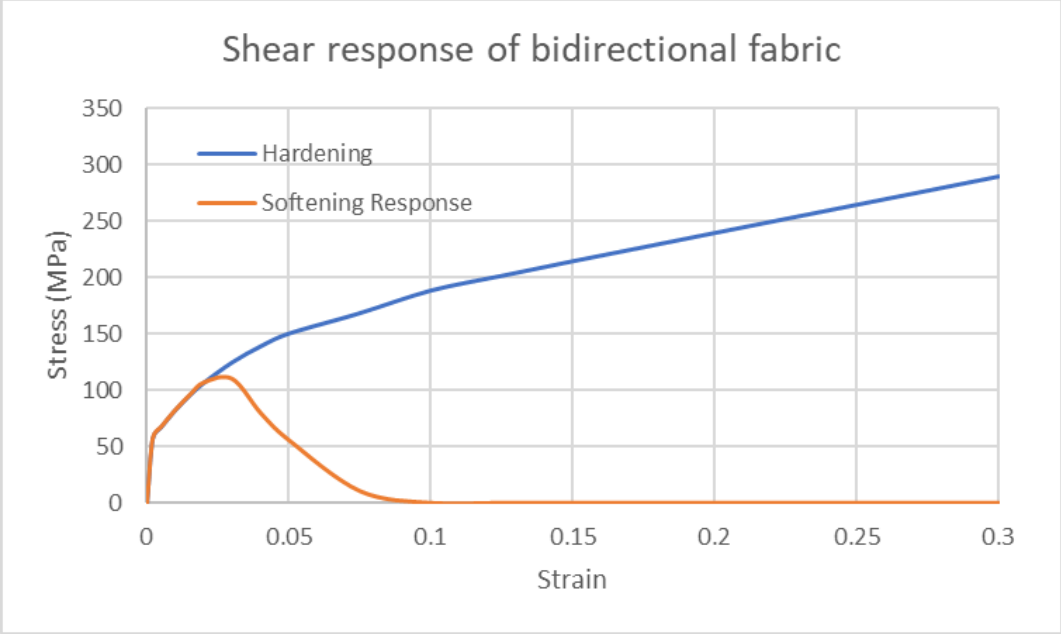


Figure 3.9 Nonlinear in-plane shear hardening curve implemented in the Abaqus Ply Fabric material model.

3.2.4. Intralaminar Damage Modelling

Intralaminar damage was modelled using the *Ply Fabric Damage* formulation available in Abaqus/Explicit module. The model distinguishes fibre-dominated and matrix-dominated failure mechanisms, allowing damage initiation and progressive stiffness degradation to be represented independently within each woven ply. The implementation adopted in the present work is described in the following sections.

Damage initiation was defined using the *Ply Fabric Damage* criterion available in Abaqus/Explicit. The formulation distinguishes five independent failure modes corresponding to fibre tensile and compressive failure in the warp and weft directions together with matrix-dominated shear failure. Fibre damage is initiated when the effective stress reaches the corresponding material strength, whereas matrix damage depends on both the effective shear stress and the accumulated equivalent plastic shear strain according to:

$$\phi_{12} = \max\left(\frac{\widehat{\sigma_{12}}}{S}, \bar{\varepsilon}^{pl} / \bar{\varepsilon}^{pl}_{max}\right) \tag{3.2}$$

where S is the shear stress for initial matrix damage, $\widehat{\sigma_{12}}$ is the effective shear stress defined as $\widehat{\sigma_{12}}=\sigma_{12}/(1-d_{12})$, $\bar{\varepsilon}^{pl}$ is the equivalent plastic strain due to shear deformation, and $\bar{\varepsilon}^{pl}_{max}$ is a specified maximum value.

The material parameters adopted in the present work are summarised in Table 3.5.

Table 3.5 Damage initiation parameters adopted for the Ply Fabric constitutive model.

Parameter	Physical meaning	Value
X1+	Warp tensile strength	804.06 MPa
X1-	Warp compressive strength	531.29 MPa
X2+	Weft tensile strength	772.77 MPa
X2-	Weft compressive strength	534.11 MPa
S12	In-plane shear strength	116.99 MPa

Following damage initiation, the progressive degradation of the woven plies was modelled using the energy-based exponential damage evolution law available in the Abaqus Ply Fabric formulation. Fibre failure is governed by the fracture energies associated with tensile and compressive loading in the warp and weft directions, whereas matrix degradation is controlled by the parameters α_{12} and d_{12max}, which define the rate and maximum level of shear stiffness

degradation. The characteristic element length is automatically incorporated into the formulation to ensure objective fracture energy dissipation and minimise mesh dependency.

The Abaqus implementation requires six material parameters: the fracture energies Gf1+, Gf1-, Gf2+ and Gf2-, together with the matrix damage parameters α_{12} and d_{12max}. The values adopted in the present work are summarised in Table 3.6.

Although the tensile damage parameters were directly adopted from the reference model, the compressive damage evolution required reformulation because the proprietary VUMAT employs a bi-linear softening law, whereas the standard *Abaqus Ply Fabric* model is based on an exponential degradation law. The procedure adopted to establish an equivalent constitutive response is presented in the following section.

Table 3.6 Damage propagation parameters adopted for the Ply Fabric constitutive model.

Parameter	Value	Unit
G_1^+	91	N/mm
G_1^-	50 (calibrated)	N/mm
G_2^+	91	N/mm
G_2^-	50 (calibrated)	N/mm
alpha_12	1	–
d_12max	0.9999	–

The constitutive model proposed by González et al. [8] employs a proprietary VUMAT in which fibre compressive failure is represented using a bi-linear softening law. In contrast, the standard Abaqus Ply Fabric formulation is based on an energy-driven exponential degradation law. Consequently, the compressive damage parameters reported in the reference study could not be transferred directly and an equivalent constitutive response had to be established.

To reproduce the reference behaviour, the original bi-linear softening law was first reconstructed using the material properties reported by González et al. [8], including the elastic modulus, compressive strength, fracture toughness, characteristic element length and

residual stress factor. This procedure enabled the complete compressive stress–strain response employed in the reference VUMAT to be obtained.

The damage initiation strain was determined from the elastic modulus and compressive strength according to:

$$\varepsilon_0 = \frac{X_1^-}{E_1} \tag{3.3}$$

where X_1^- is the compressive strength and E_1 is the elastic modulus in the fibre direction.

The stress corresponding to the change in slope of the bi-linear softening law was determined from the residual stress factor fX:

$$\sigma_i = X_1^- f_x \tag{3.4}$$

Table 3.7 Parameters employed for the reconstruction of the reference bi-linear compressive softening law

Description	Symbol	Value	Unit
Elastic modulus	E_1	59540	MPa
Compressive strength	X_1^-	531.29	MPa
Compressive fracture toughness	Gf_1^-	10000	N/mm
Characteristic element length	lc	1.5	mm
Residual stress factor	fX	0.2	–
Damage initiation strain	$\varepsilon_o = X_1^- / E_1$	0.00892	–

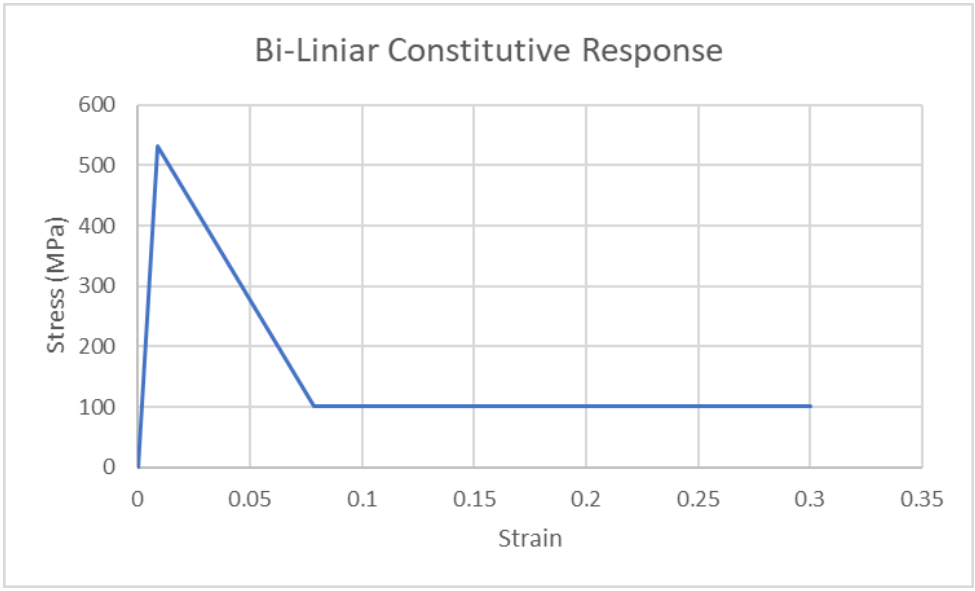


Figure 3.10 Reconstruction of the bi-linear compressive softening law proposed by González et al.

The reconstructed response shows that the fracture toughness adopted in the reference model (Gf=10,000 N/mm) produces a very gradual post-peak degradation, maintaining a significant residual load-carrying capacity over the strain range typically reached during low-velocity impact. This behaviour was intentionally introduced in the original VUMAT to reproduce the progressive crushing response of woven composite plies.

To obtain an equivalent response compatible with the standard Abaqus formulation, the compressive behaviour was reformulated using the exponential damage evolution law implemented in the Ply Fabric material model. The post-peak response is controlled by the fracture energy, which therefore became the principal calibration parameter during the present work. An initial fracture toughness of 50 N/mm was adopted as the starting point for the calibration, producing a steeper post-peak degradation while maintaining progressive energy dissipation.

Figure 3.11 compares the reconstructed bi-linear response with the exponential constitutive law implemented in Abaqus. Although the exponential formulation cannot exactly reproduce the reference bi-linear behaviour, it provides a physically consistent representation within the limitations of the standard Ply Fabric model and preserves the fracture-energy-based damage evolution required for the impact simulations.

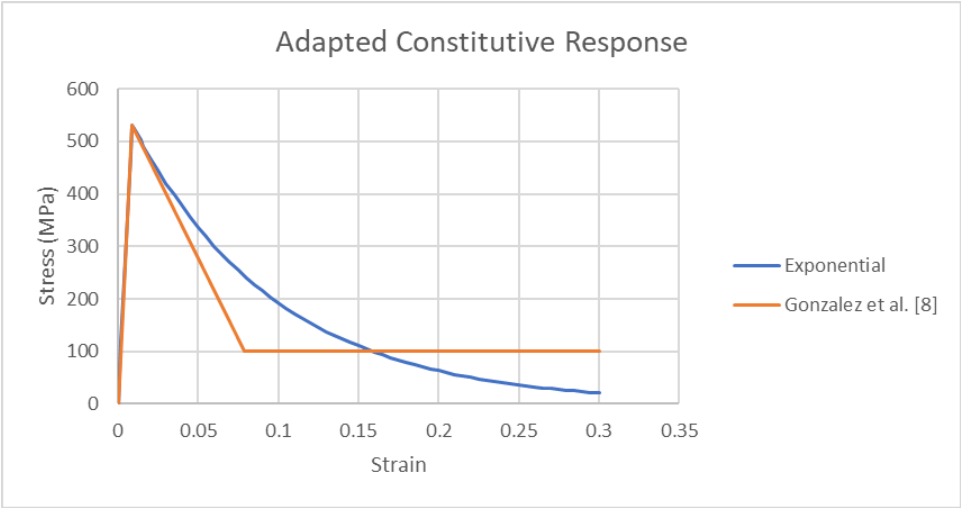


Figure 3.11 Comparison between the reference bi-linear softening law and the exponential softening law implemented in the present Abaqus model.

Finally, the maximum compressive plastic strain defined in the Ply Fabric Failure criterion was selected to exceed the strain at which the exponential stress approaches zero. This ensured that the post-peak response was governed by the fracture energy rather than by premature material deletion, allowing the complete exponential damage evolution to develop during the simulations.

The final stage of the intralaminar damage model was defined using the Ply Fabric Failure criterion available in Abaqus/Explicit. This formulation specifies the limiting strains beyond which the material point is removed from the analysis, preventing excessive element distortion after the degradation process has been completed.

The failure limits were selected to ensure that element deletion occurred only after the exponential damage evolution law had fully developed. In particular, the maximum compressive strain was adjusted to exceed the strain corresponding to complete stress degradation, allowing the fracture energy prescribed in the damage evolution law to be fully dissipated before material removal.

The failure parameters adopted in the present work are summarised in Table 3.8.

Table 3.8 Fabric failure parameters adopted for the Ply Fabric constitutive model.

Parameter	Symbol	Value	Unit
Maximum tensile strain	ε_1^T,max	0.05	–
Maximum compressive strain	ε_1^c,max	0.12	–
Maximum plastic shear strain	γ_{12}^P,max	0.12	–

In addition to the constitutive material definition, the SC8R continuum shell formulation requires the specification of the thickness modulus and the transverse shear stiffness, which define the out-of-plane behaviour of the laminate.

A value of 10,000 MPa for was adopted for the thickness modulus to provide a realistic through-thickness modulus while maintaining numerical stability throughout the explicit impact simulations.

The transverse shear stiffness was calculated according to the Abaqus continuum shell formulation,

$$K_{ts} = k\, G_{13}\, t \tag{3.5}$$

where (k=5/6) is the shear correction factor, G_{13} is the transverse shear modulus and *t* is the thickness of the continuum shell section. Since each shell section represents a single ply, the ply thickness (0.353 mm) was used in the calculation rather than the total laminate thickness. Substituting the material properties used in the present work,

$$K_{ts} = \frac{5}{6} \times 4666 \times 0.353 = 1373.8 \ \text{N/mm} \tag{3.6}$$

resulting in the transverse shear stiffness adopted in the Abaqus shell section.

3.2.5. Cohesive Interface Modelling

Interlaminar delamination was represented by inserting cohesive elements between every pair of adjacent plies, resulting in eleven cohesive interfaces through the laminate thickness. This discretisation enabled delamination to initiate and propagate independently at each interface during the impact event.

The cohesive material properties were adopted directly from the reference model proposed by González et al. [8]. Damage initiation was governed by a quadratic nominal stress criterion, while crack propagation was described using an energy-based mixed-mode traction–separation law based on the Benzeggagh–Kenane (BK) criterion.

The complete set of cohesive parameters adopted in the present work is summarised in Table 3.9.

Table 3.9 Cohesive Interface properties adopted for the Ply Fabric constitutive model.

Property	Symbol	Value	Unit
Cohesive element type	–	COH3D8	–
Number of cohesive interfaces	–	11	–
Normal penalty stiffness	Knn	83100	MPa/mm
First shear penalty stiffness	Kss	83100	MPa/mm
Second shear penalty stiffness	Ktt	83100	MPa/mm
Normal cohesive strength	t_n^o	55.47	MPa
First shear cohesive strength	t_s^o	116.99	MPa
Second shear cohesive strength	t_t^o	116.99	MPa
Mode I fracture toughness	GIc	1.01	N/mm
Mode II fracture toughness	GIIc	2.45	N/mm
Mode III fracture toughness	GIIIc	2.45	N/mm
Benzeggagh–Kenane exponent	ηBK	1.88	–

3.2.6. Contact Interactions

Contact interactions were defined using the General Contact algorithm available in Abaqus/Explicit. A hard contact formulation was adopted in the normal direction to prevent surface penetration while allowing separation after unloading. In the tangential direction, a penalty friction formulation with a constant coefficient of friction of 0.3 was assigned to all contact interactions.

The same contact definition was applied throughout the numerical model, including the interactions between the impactor and the laminate, the laminate and the support fixture, and the laminate and the clamping system.

3.2.7. Boundary and Load Conditions

The boundary conditions were defined to reproduce the experimental impact configuration reported by González et al. [8]. The support fixture was modelled as a rigid body and fully constrained throughout the simulation.

To reproduce the experimental clamping system, an initial vertical displacement of 2.5×10^{-3} mm, as defined in González et al. [8], was prescribed to the four clamping pads towards the laminate, generating a small preload that ensured continuous contact prior to impact. The hemispherical impactor was modelled as a rigid body with a total mass of 5 kg and an initial velocity of 4 m/s, corresponding to an impact energy of approximately 40 J:

$$E = \frac{1}{2}\, m\, v^2 \tag{3.7}$$

where m is the impactor mass and v is the initial impact velocity.
The impact event was simulated using the Dynamic Explicit solver with a total analysis time of 0.01 s, which was sufficient to capture the complete impact event and the subsequent damage evolution.

3.2.8. Output Requests

Field and history output requests were defined to evaluate both the damage mechanisms developed within the laminate and the global impact response.

For the cohesive interfaces, the SDEG variable was requested to identify the initiation and propagation of delamination and to determine the final delaminated area. In addition, the *Ply Fabric* damage variables associated with fibre tensile damage, fibre compressive damage and matrix shear damage were recorded to assess the intralaminar failure mechanisms.

The internal and kinetic energies were monitored throughout the analysis to verify the energy balance of the explicit simulation. Finally, the acceleration and displacement histories of the impactor were extracted. The impact force was subsequently calculated from the acceleration history using Newton's second law and combined with the displacement history to obtain the load–displacement response.

3.2.9. Model Calibration

The numerical model proposed by González et al. [8] was adopted as the reference configuration for the Abaqus implementation. However, several modifications were required because the original model employed a proprietary VUMAT, whereas the present work was developed exclusively using the standard material models available in Abaqus/Explicit libraries.

The calibration process was therefore restricted to the parameters directly affected by this change in constitutive formulation. The laminate geometry, stacking sequence, boundary conditions, contact definitions and cohesive interface properties were maintained identical to the reference model, while only the intralaminar constitutive response was adapted.

The principal modifications introduced during the calibration process were:

- reconstruction of the nonlinear in-plane shear hardening curve in a tabulated format compatible with the Ply Fabric formulation;
- extension of the hardening curve beyond the experimentally characterised strain range to avoid numerical extrapolation during the impact simulations;
- reformulation of the compressive damage evolution from the original bi-linear softening law to the exponential degradation law available in Abaqus;
- definition of the continuum shell section parameters, including the thickness modulus and transverse shear stiffness;

- adjustment of the Ply Fabric failure limits to ensure complete energy dissipation prior to element deletion.

3.3. Adaptive ERR-Cohesive Large Element Model (LS-DYNA®)

Alongside the Abaqus model developed using the built-in Ply Fabric constitutive formulation, a model was implemented on LS-DYNA based on the adaptive ERR–cohesive framework developed by Daniel et al. [16] and described in Section 2.3.2. The present chapter focuses on the implementation of this methodology for the simulation of low-velocity impact, while the theoretical background of the adaptive formulation will not be repeated.

3.3.1. Laminate Material Definition

The same laminate architecture employed in the Abaqus model was adopted, consisting of a twelve-ply woven CFRP laminate with a stacking sequence of $[(0/45)_3]_s$ and an individual ply thickness of 0.353 mm.

The orthotropic elastic properties were introduced through the material card *MAT_USER_DEFINED_MATERIAL_MODELS. Following the LS-DYNA convention, the Poisson's ratios are defined as ν_{21}, ν_{31} and ν_{32}. The material properties used in the simulations are listed in Table 3.2.

The material properties correspond to the HexForce G0926/RTM6 woven CFRP system used throughout this work and are consistent with the reference impact model reported by González et al. [8].

3.3.2. Model Organisation

The LS-DYNA numerical model was organised using a modular structure based on include files, allowing each component of the finite element model to be defined independently. This organisation facilitates model development, parameter modification and debugging, while enabling individual files to be updated without affecting the remaining model definition.

The main input file references a series of include files responsible for defining the analysis controls, geometry, material properties, contact interactions, loading conditions and output requests. The principal include files employed in the present work are summarised in Table 3.10.

Table 3.10 Main include files employed in the LS-DYNA model.

Include file	Description
000_CONTROLS_AND_DATABASE_R14.k	Analysis control cards, solver settings and database output requests.
02_Rigid_Parts.k	Definition of the rigid bodies, including the impactor and supporting fixture.
03_MAT_ADAPT_LAMINATE.k	Laminate material definition and adaptive ERR–cohesive parameters.
03_MAT_ADAPT_LAMINATE_UNLS.k	Alternative laminate material definition used for different numerical configurations.
04_CONTACTS.k	Contact definitions between all interacting components.
05_BOUNDARY_CONDITIONS.k	Boundary conditions applied to the model.
06_LOADS_AND_CURVES.k	Loading definitions and prescribed load/displacement curves.
07_PART_AND_SEGMENT_SETS.k	Definition of part and segment sets used for contacts, boundary conditions and post-processing.
08_ELEMENTS_SOLID.k	Solid element connectivity of the finite element mesh.
09_NODES.k	Nodal coordinates defining the finite element mesh.

Particular attention was given to the MAT_ADAPT_LAMINATE include file, which contains the laminate definition together with the parameters controlling the adaptive ERR–cohesive formulation. This file also specifies the interfaces selected for enrichment through the corresponding ENRICH parameters, allowing different enrichment configurations to be analysed without modifying the finite element model.

3.3.3. Mesh Discretisation

The laminate was discretised using a structured in-plane mesh with a uniform element size of 3 × 3 mm. Unlike the Abaqus implementation, where the laminate is discretised through the thickness using continuum shell and cohesive elements, the adaptive LS-DYNA formulation represents the complete laminate using a single solid-shell element through the thickness. Consequently, only the in-plane mesh discretisation must be defined explicitly.

According to the validation studies performed during the development of the adaptive ERR–cohesive framework, the formulation provides mesh-independent predictions for element sizes between 2 and 5 mm. The selected element size of 3 mm therefore lies within the recommended range, ensuring accurate delamination prediction while maintaining a low computational cost.

Unlike conventional layer-wise finite element models, the complete laminate is represented using a single adaptive solid-shell element through the thickness, see Figure 3.12. The stacking sequence, individual ply thicknesses, orthotropic material properties and potential delamination interfaces are internally defined within the MAT_ADAPT_LAMINATE material card, eliminating the need to explicitly discretise each ply and interface.

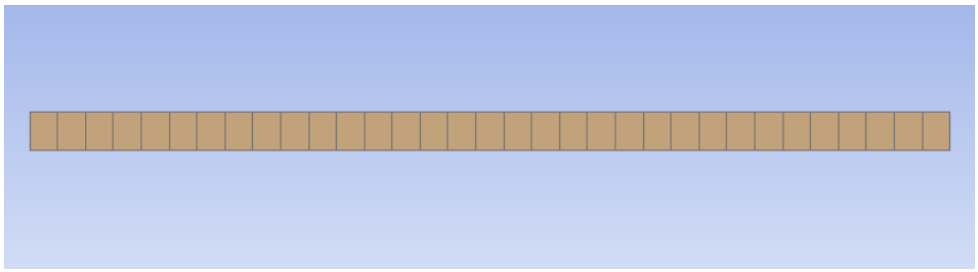


Figure 3.12 Laminate through-thickness definition

The laminate consists of twelve woven CFRP plies arranged in a symmetric $[(0/45)_3]_s$ stacking sequence, resulting in eleven potential interlaminar interfaces where delamination may occur. Within the adaptive formulation, each ply is assigned its corresponding material orientation and thickness, while the laminate architecture is reconstructed internally by the user-defined material model. Consequently, although the finite element mesh contains only one element through the thickness, the constitutive response is evaluated independently for

each ply, preserving the laminate stacking sequence and enabling both intralaminar and interlaminar damage mechanisms to be represented.

Potential delamination interfaces are defined between every pair of adjacent plies and are internally numbered from the upper to the lower surface of the laminate. These interface identifiers are subsequently used to define the enriched interfaces through the adaptive formulation.

The interfaces selected for enrichment are specified in the MAT_ADAPT_LAMINATE include file through the parameters ENRICH1 to ENRICH5, each corresponding to one laminate interface. Since the current implementation of the adaptive framework allows a maximum of five enriched interfaces to be activated within a single simulation, different enrichment configurations were investigated throughout this work by modifying the interface numbers assigned to these parameters.

3.3.4. Adaptive Delamination Parameters

The adaptive laminate definition described in Section 3.3.3 was complemented by a set of parameters controlling the interlaminar damage formulation implemented in the user-defined subroutine. These parameters define the failure criterion, fracture properties and numerical settings governing the adaptive ERR–cohesive formulation, while the selection of the enriched interfaces was performed independently through the ENRICH parameters presented in the previous section.

The interlaminar fracture behaviour is characterised by the critical fracture toughness under Mode I and Mode II loading, represented by the parameters G_{IC} and G_{IIC}, respectively. Mixed-mode delamination propagation is evaluated using the Benzeggagh–Kenane (BK) fracture criterion, whose exponent is defined by the parameter XMU. Together, these parameters determine the critical Energy Release Rate required for crack propagation under mixed-mode loading.

The material card also defines the interlaminar tensile strength (T) and shear strength (S), which govern the initiation of the interlaminar damage process. Additional numerical

parameters controlling the adaptive formulation, including the interface thickness parameter (ET), damage evolution (GAMMA) and the selected failure criterion (INTFAIL), were kept unchanged throughout the study. The values adopted in the present work are summarised in Table 3.11.

Table 3.11 Adaptive delamination parameters defined in the MAT_ADAPT_LAMINATE material card.

Parameter	Value	Description
INTFAIL	4	Interlaminar failure criterion
ET	0.6	Interface thickness parameter
GIc	1.01 N/mm	Mode I fracture toughness
GIIc	2.45 N/mm	Mode II fracture toughness
XMU	-2	Benzeggagh–Kenane exponent
T	55.47 MPa	Interlaminar tensile strength
S	116.99 MPa	Interlaminar shear strength
GAMMA	1	Damage evolution parameter

3.3.5. Intralaminar Damage Modelling

Unlike the baseline adaptive model presented in the previous sections, the final LS-DYNA implementation incorporates an intralaminar damage formulation through the user-defined material model developed by Martín-Santos et al. [29]. This constitutive model is formulated within the framework of Continuum Damage Mechanics (CDM) and was originally developed for woven fabric-reinforced composites. The formulation combines orthotropic elasticity, progressive fibre damage and nonlinear in-plane shear plasticity within a single constitutive law, enabling both the elastic response and the degradation of the laminate to be represented during impact loading.

The constitutive model considers four independent fibre-related failure mechanisms corresponding to tensile and compressive failure in both the warp (1-direction) and weft (2-direction). Damage initiation is evaluated using maximum-stress loading functions defined independently for each material direction. Tensile failure depends only on the effective stress acting along the corresponding fibre direction, whereas compressive failure additionally

accounts for the influence of transverse compression and shear stresses through biaxial interaction terms. Once the damage criterion is satisfied, the material stiffness progressively degrades according to a bilinear cohesive damage law regularised using the Crack Band Model, ensuring that the dissipated fracture energy remains essentially independent of the finite element size.

In addition to the fibre failure mechanisms, the constitutive formulation incorporates a nonlinear in-plane shear response represented by an exponential isotropic hardening law. The shear behaviour evolves as a function of the accumulated plastic shear strain, allowing the characteristic nonlinear response of woven composites to be reproduced prior to failure without explicitly modelling matrix cracking.

The material definition adopted in the present work is based on the woven CFRP properties reported by González et al. [8], including the elastic constants, strength values and fracture toughness parameters previously presented in Table 3.2. However, the user-defined constitutive model proposed by Martín-Santos et al. [29] requires several additional parameters governing the bilinear fibre damage laws and the nonlinear shear hardening formulation. Since these parameters are not provided in the reference impact model of González et al. [8], they were incorporated to complete the constitutive definition required by the VUMAT. The additional constitutive parameters employed in the present work are summarised in Table 3.12.

Table 3.12 Additional constitutive parameters required by the LS-DYNA user-defined material model.

Parameter	Symbol	Value
Tensile softening slope (warp)	H1T	4495.84 MPa/mm
Compressive softening slope (warp)	H1C	3464.21 MPa/mm
Tensile softening slope (weft)	H2T	4152.73 MPa/mm
Compressive softening slope (weft)	H2C	3501.08 MPa/mm
Residual stress factor (warp tension)	fX1T	0.19
Residual stress factor (warp compression)	fX1C	0.19
Residual stress factor (weft tension)	fX2T	0.19
Residual stress factor (weft compression)	fX2C	0.19
Shear yield stress	SLP	50 MPa
Exponential hardening coefficient	Ce	89.6
Exponential hardening exponent	CTe	36.9
Linear hardening coefficient	Cl	500

3.3.6. Output Requests

The output requests were defined to evaluate both the global structural response of the laminate and the evolution of the interlaminar and intralaminar damage mechanisms during the impact event. Standard LS-DYNA database outputs were employed to extract the contact force, impactor displacement, energy balance and nodal displacements, enabling a direct comparison with the Layer-wise Model with Cohesive Interfaces and the experimental results.

In addition to the conventional output variables, the adaptive ERR–cohesive subroutine provides a set of history variables specifically developed to monitor delamination propagation. Five state variables (21–25) are assigned to the enriched interfaces and indicate the delamination state of each individual interface considered during a given simulation. Since a maximum of five interfaces can be enriched simultaneously, these variables provide the evolution of delamination independently for each enriched interface.

Furthermore, state variable 57 stores the projected delaminated area obtained by combining the contribution of all enriched interfaces. This variable was used throughout the present work to quantify the overall delamination area and to compare the numerical predictions with the experimental observations and the Layer-wise Model with Cohesive Interfaces.

Following the incorporation of the intralaminar damage formulation, additional history variables from the user-defined material model were also requested. State variables 67 and 68 correspond to the fibre damage variables in the first and second material directions, respectively, and report the maximum damage value through the laminate thickness. These variables were employed to evaluate the spatial distribution and severity of fibre degradation during impact. In addition, state variable 71 represents the accumulated shear plasticity, also reported as the maximum value through the laminate thickness, providing a measure of the nonlinear shear response associated with the matrix-dominated behaviour. Together, these variables enable the evolution of intralaminar damage to be analysed alongside the interlaminar delamination predicted by the adaptive ERR–cohesive methodology.

THIS PAGE WAS INTENTIONALLY LEFT BLANK

4. RESULTS AND DISCUSSION

4.1. Validation Strategy and Scope

This chapter presents the validation of the numerical models against the experimental low-velocity impact tests. The comparison focuses on the main quantities used to assess the structural response of the laminate, namely the force–displacement curve, the energy response and the predicted delamination.

The results are presented progressively. First, the elastic response is evaluated to verify the accuracy of the structural model before damage initiation. Subsequently, the complete layer-wise Abaqus model with cohesive interfaces is analysed, focusing on its ability to reproduce the global impact response and the experimentally observed delamination. Finally, the adaptive ERR–cohesive LS-DYNA model is assessed and compared with the Abaqus approach, highlighting the capabilities and limitations of both modelling strategies.

4.2. Initial Elastic Response Validation

Before analysing the damage mechanisms predicted by each modelling approach, it is essential to verify that both numerical models accurately reproduce the elastic response of the laminate. The comparison presented in this section focuses on the initial stage of the impact event, prior to the initiation of significant damage, where the global response is governed by the elastic properties of the laminate, the contact definition and the applied boundary conditions. Although the Layer-wise Model with Cohesive Interfaces already includes cohesive interfaces, these remain inactive during the elastic stage and therefore do not influence the structural response. Consequently, this comparison provides a direct assessment of the consistency of the elastic formulations implemented in both numerical models.

Figure 4.1 compares the initial force–displacement response obtained from the experimental test, the numerical model reported by González et al. [8], the Layer-wise Model with Cohesive Interfaces, and the baseline Adaptive ERR–Cohesive Large-Element Model.

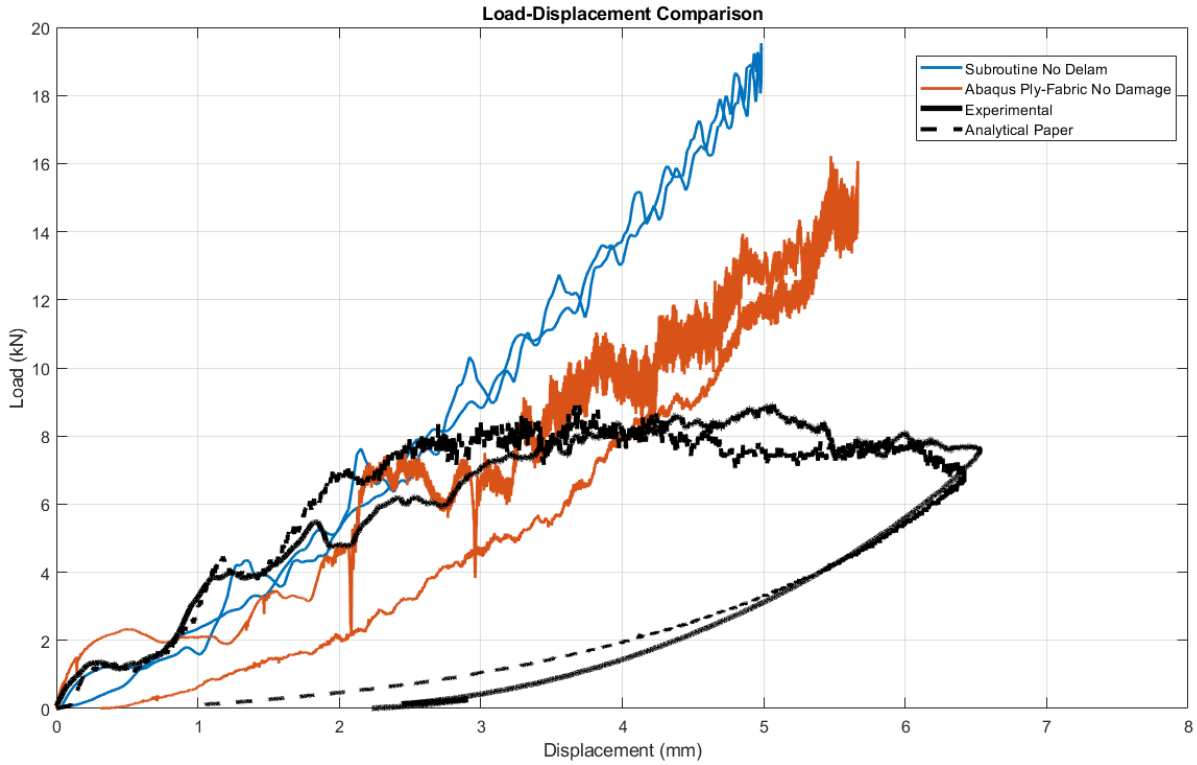


Figure 4.1 Comparison of the elastic force–displacement response obtained from the experimental test, the analytical reference model and the numerical models.

As shown in Figure 4.1, both numerical models accurately reproduce the initial stiffness of the laminate and follow the experimental response closely throughout the elastic loading stage. The agreement obtained confirms that the elastic properties, laminate configuration and contact definitions adopted in both models provide a consistent representation of the structural behaviour prior to damage initiation. Since the cohesive interfaces remain inactive during this stage, the similarity between both responses demonstrates that the structural formulations are equivalent before interlaminar damage develops.

To further investigate the initial contact behaviour, an enlarged view of the beginning of the force–displacement response is presented in Figure 4.2.

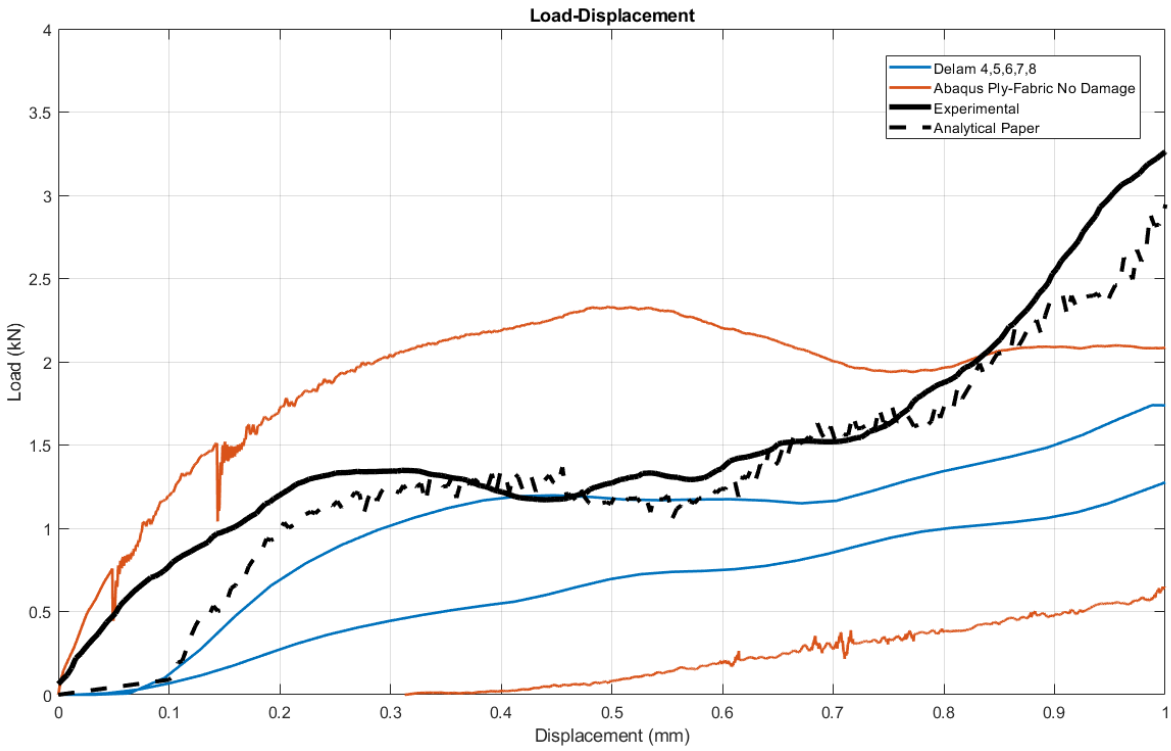


Figure 4.2 Detailed comparison of the initial contact stage between the experimental response, the analytical reference solution and the numerical models.

The enlarged view reveals small differences in the onset of the contact response. The experimental curve exhibits a slightly steeper increase in load, whereas both numerical models show a more progressive contact development. Since no damage has yet initiated, these discrepancies cannot be attributed to the constitutive or damage formulations. Instead, they are more likely associated with slight differences in the representation of the support conditions, including the clamping configuration, the applied clamping pressure and the initial positioning of the impactor relative to the laminate. Although these effects influence the establishment of contact during the first stages of the impact event, they have only a minor effect on the subsequent structural response.

Although the validation presented in this section is restricted to the elastic stage, the complete force–displacement responses, taking into account the interlaminar behaviour, are shown in Figure 4.3 to illustrate the influence of introducing adaptive delamination into the Adaptive ERR–Cohesive Large-Element Model.

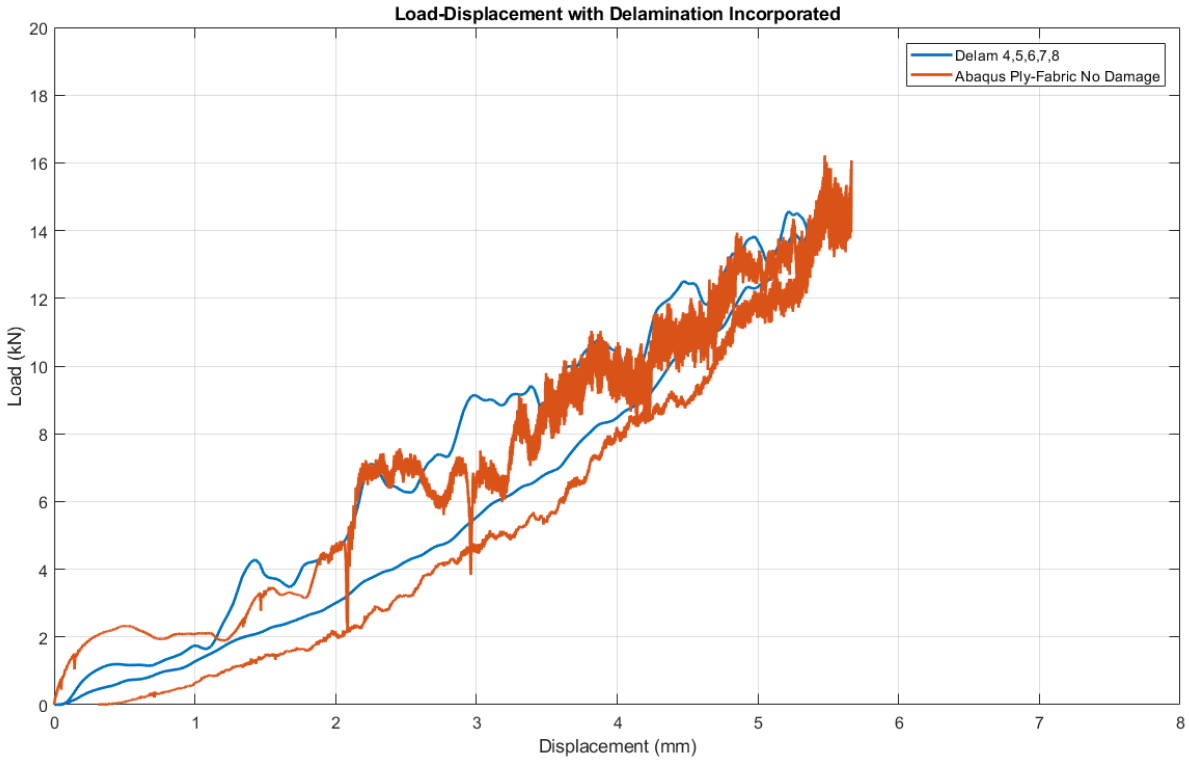


Figure 4.3 Complete force–displacement response comparing the Layer-wise Model with Cohesive Interfaces and the Adaptive ERR–Cohesive Large-Element Model after the implementation of adaptive delamination.

As observed in Figure 4.3, the baseline Adaptive ERR–Cohesive Large-Element Model predicts a significantly stiffer response than the Layer-wise Model with Cohesive Interfaces as the impact progresses. This difference arises because the adaptive delamination formulation has not yet been activated in the baseline model, whereas the Layer-wise Model with Cohesive Interfaces already allows the initiation and propagation of interlaminar delamination through the cohesive interfaces. Consequently, once delamination starts to develop, the two models no longer represent the same physical problem. After activating the adaptive ERR–cohesive formulation, the predicted response becomes remarkably similar to that of the Layer-wise Model with Cohesive Interfaces, see Figure 4.3, indicating that the discrepancies observed beyond the initial elastic stage are primarily associated with the inclusion of interlaminar delamination rather than with the underlying elastic structural formulation.

Overall, the results presented in this section demonstrate that both numerical models provide a consistent prediction of the laminate response during the elastic stage. Furthermore, the

incorporation of adaptive delamination enables the Adaptive ERR–Cohesive Large-Element Model to reproduce the global behaviour of the Layer-wise Model with Cohesive Interfaces beyond damage initiation, providing confidence in the implementation of the proposed adaptive methodology before proceeding with the detailed validation against the experimental results.

4.3. Layer-wise Model with Cohesive Interface Behaviour and Intralaminar Damage

4.3.1. Force–displacement response

The global force–displacement response predicted by the Layer-wise Model with Cohesive Interfaces was compared with the experimental results and the analytical reference model proposed by González et al. [8] to evaluate the capability of the numerical model to reproduce the structural behaviour of the laminate throughout the impact event. The comparison is presented in Figure 4.4.

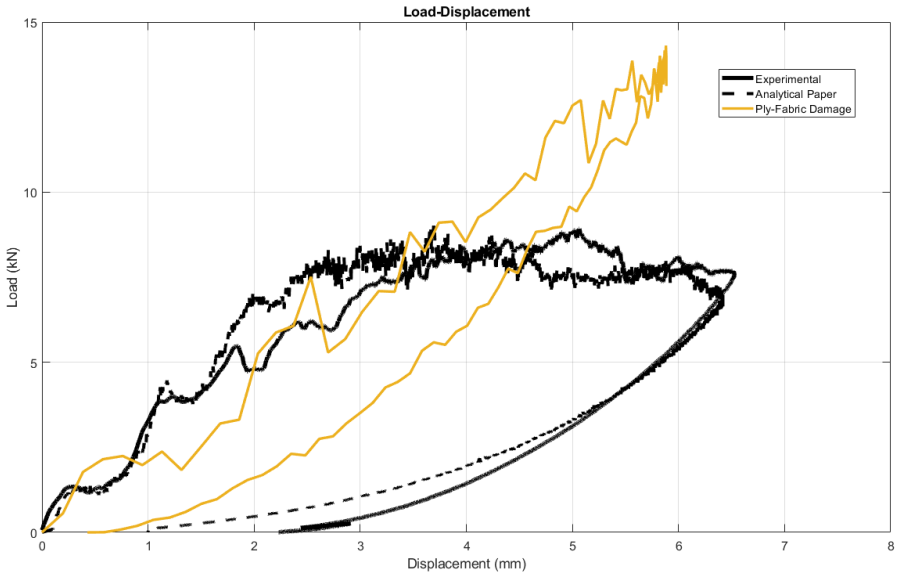


Figure 4.4 Comparison of the complete force–displacement response obtained from the experimental test, the analytical reference model and the Layer-wise Model with Cohesive Interfaces.

The numerical model reproduces the overall evolution of the impact response, correctly capturing the initial stiffness of the laminate as well as the progressive increase in contact load during the first stages of the impact event. The onset of non-linearity also occurs at a displacement comparable to that observed experimentally, indicating that the elastic properties, laminate configuration and contact definition adopted in the model provide a realistic representation of the structural behaviour prior to significant damage development.

A more detailed comparison of the initial loading stage is presented in Figure 4.5.

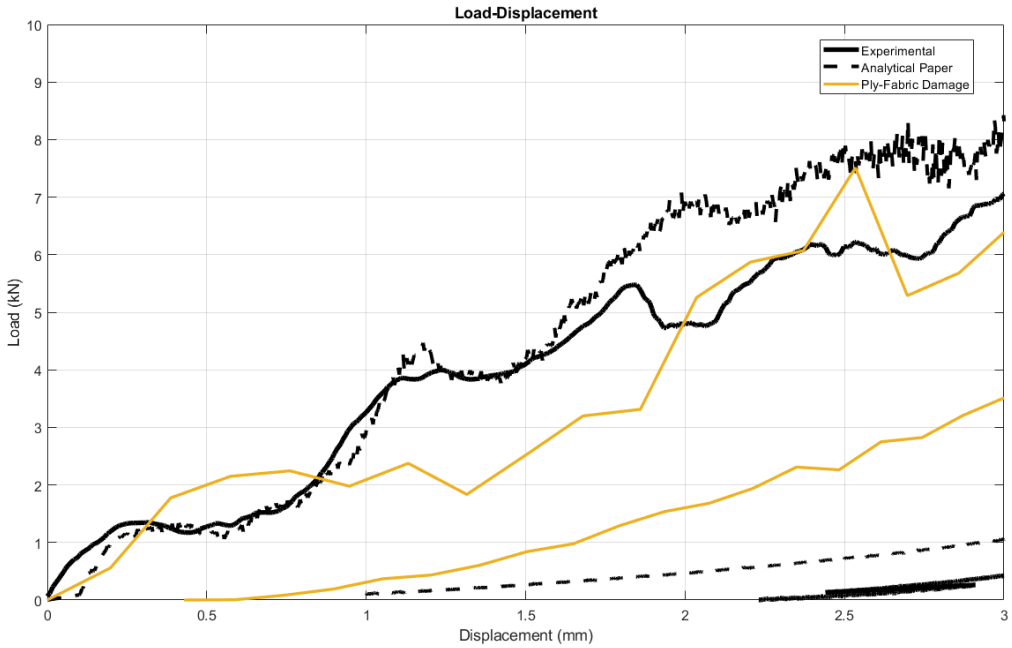


Figure 4.5 Detailed comparison of the initial loading stage of the force–displacement response.

The enlarged view confirms the good agreement between the numerical prediction and the experimental response during the early stages of loading. Small local differences can be observed in the establishment of contact, which are attributed to minor differences in the representation of the support conditions and contact interfaces. Nevertheless, these discrepancies remain limited and do not significantly affect the global stiffness of the laminate.

Beyond the initial loading stage, the numerical response progressively deviates from the experimental behaviour. While the experimental curve reaches a maximum load of

approximately 8–9 kN before exhibiting a progressive reduction associated with damage development, the numerical model continues to increase almost monotonically, reaching loads above 13 kN. This behaviour indicates that the laminate retains a higher structural stiffness than observed experimentally after the onset of damage.

The absence of a significant load reduction suggests that the degradation mechanisms represented in the model are not sufficient to reproduce the stiffness loss measured during the experiments. Although the cohesive interfaces successfully initiate interlaminar delamination, the global response indicates that additional damage mechanisms contribute to the experimental behaviour. In particular, intralaminar damage is expected to play an important role in reducing the structural stiffness of the laminate as the impact progresses. Consequently, the numerical model overestimates the load-carrying capacity during the later stages of the impact event.

Despite these discrepancies, the model correctly predicts the initial elastic response and the transition towards damage initiation, providing a reliable basis for the subsequent evaluation of the energy response and the delamination predictions presented in the following sections.

4.3.2. Energy response

The internal energy evolution predicted by the Layer-wise Model with Cohesive Interfaces was compared with the analytical reference model to evaluate the capability of the numerical model to reproduce the energy absorption during the impact event. Unlike the force–displacement response, the internal energy provides direct information about the balance between the elastic strain energy temporarily stored within the laminate and the irreversible energy dissipated through damage mechanisms.

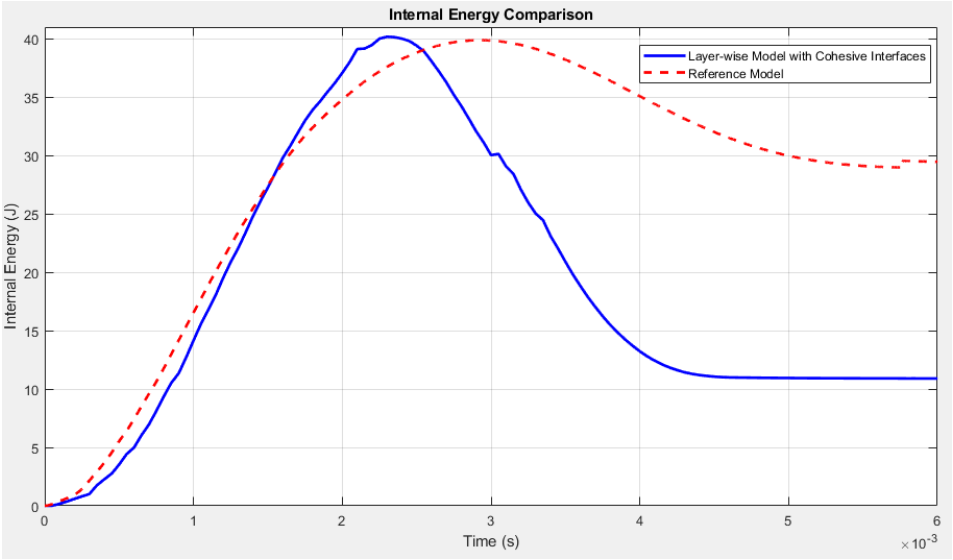


Figure 4.6 Comparison of the internal energy evolution predicted by the Layer-wise Model with Cohesive Interfaces and the analytical reference model.

As shown in Figure 4.6, both models exhibit a very similar evolution during the initial loading stage. The internal energy increases almost identically up to approximately 1.7–2.0 ms, indicating that both models store a comparable amount of elastic strain energy before significant damage develops. Furthermore, both approaches predict a maximum internal energy close to the initial impact energy of 40 J, confirming that the impact event is correctly represented and that the laminate absorbs nearly the entire kinetic energy of the impactor during the loading phase.

The main differences appear immediately after the peak energy is reached. While the analytical reference model exhibits only a gradual reduction in internal energy, the Layer-wise Model with Cohesive Interfaces shows a much more pronounced decrease, stabilizing at approximately 11 J, compared with approximately 29 J in the reference solution. This behaviour indicates that the numerical model releases a considerably larger fraction of the energy stored during loading, resulting in a significantly lower amount of residual energy remaining within the laminate after impact.

To further investigate the origin of these differences, the intralaminar damage predicted in the outer plies of the laminate was analysed at the end of the impact event.

The damage maps presented reveal that intralaminar degradation remains highly localized around the impact point. In the 0° ply (Figure 4.7), fibre failure is concentrated within a narrow band aligned with the fibre direction, with almost no lateral propagation beyond the immediate impact region. In contrast, the 45° ply (Figure 4.8) exhibits a slightly more distributed fibre damage pattern surrounding the impact location, although the damaged region remains confined to a relatively small area. The shear damage predicted in the 45° ply (Figure 4.9) follows a similar trend, remaining localized around the impact point without significant propagation across the ply. Overall, both fibre and shear damage are restricted to a very limited region beneath the impactor, while the majority of the laminate remains essentially undamaged.

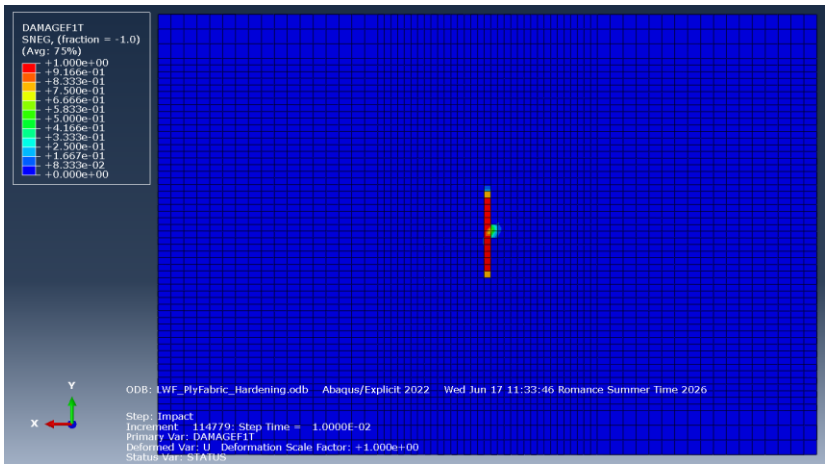


Figure 4.7 Predicted intralaminar damage at the end of the impact simulation: fibre damage in the outer 0° ply

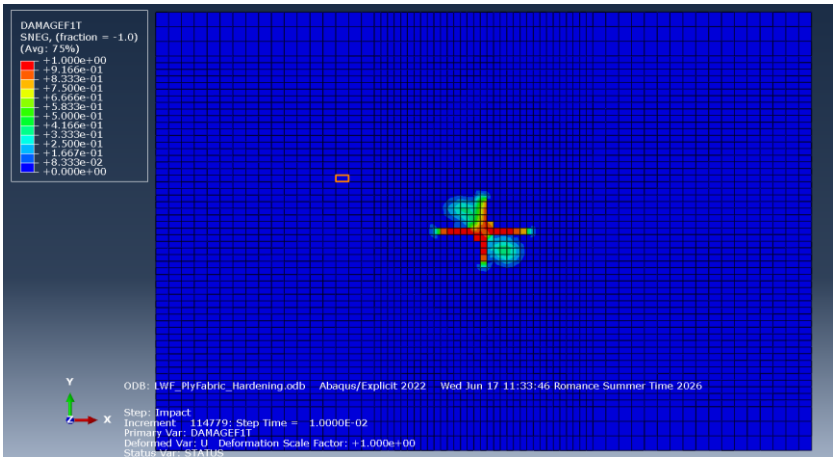


Figure 4.8 Predicted intralaminar damage at the end of the impact simulation: fibre damage in the outer 45° ply

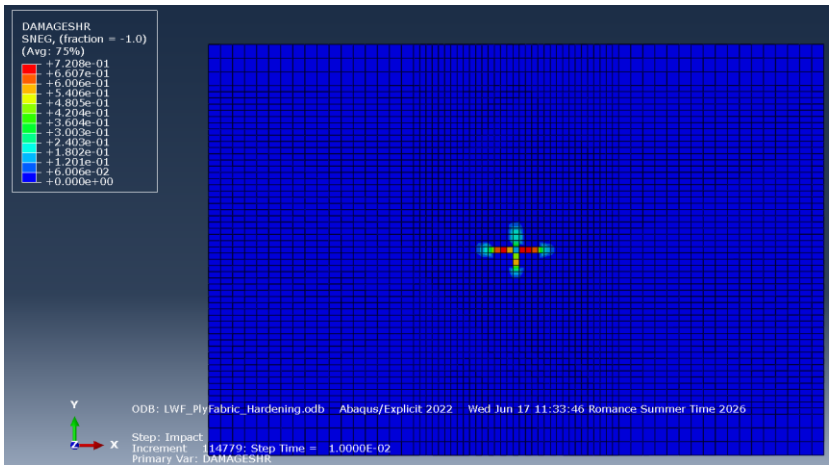


Figure 4.9 Predicted intralaminar damage at the end of the impact simulation: shear damage

The limited spatial extent of the predicted intralaminar damage provides a plausible explanation for the internal energy response shown in Figure 4.6. Since irreversible material degradation is concentrated within a relatively small volume of the laminate, only a limited fraction of the impact energy is permanently dissipated through ply failure. Consequently, a larger proportion of the strain energy accumulated during loading remains elastically recoverable and is released during unloading, leading to the substantially lower residual internal energy predicted by the numerical model. This interpretation is also consistent with the force–displacement response discussed in the previous section, where the laminate retains a higher load-carrying capacity after damage initiation.

An additional factor that may contribute to the observed differences is the discretisation strategy adopted for the laminate. The analytical reference model employs cohesive surface interactions, allowing each ply to be meshed independently according to its fibre orientation. Consequently, the ±45° plies are discretized using elements aligned with the fibre direction, providing a mesh that better follows the local material axes and the expected damage propagation paths. In contrast, the Layer-wise Model with Cohesive Interfaces employs cohesive elements between adjacent plies. This formulation requires node-to-node compatibility across every interface, forcing all plies to share an identical mesh regardless of their fibre orientation. As a result, the ±45° plies cannot be discretized with elements aligned to the fibre direction. Although this approach ensures mesh compatibility and simplifies the

implementation of the cohesive interfaces, it may influence the local stress distribution, the development of intralaminar damage and, consequently, the predicted energy dissipation.

Overall, the Layer-wise Model with Cohesive Interfaces accurately reproduces the accumulation of internal energy during the loading stage and predicts a realistic maximum energy value. However, the unloading response exhibits a greater recovery of elastic strain energy than the analytical reference model, resulting in a lower residual internal energy after impact. The present results suggest that this behaviour is associated with the combined effect of the limited intralaminar degradation predicted by the constitutive formulation and the mesh constraints imposed by the use of cohesive elements between adjacent plies.

4.3.3. Delamination prediction

The primary objective of the Layer-wise Model with Cohesive Interfaces is to accurately reproduce the initiation and propagation of interlaminar delamination during low-velocity impact. Therefore, beyond the comparison of the global structural response, it is essential to evaluate the capability of the model to predict the size and morphology of the delaminated region.

Figure 4.10 compares the projected delaminated area obtained from the numerical model with that reported in the analytical reference model. Overall, an excellent agreement is observed in both the size and the overall shape of the delaminated region. The numerical prediction successfully reproduces the nearly circular damage morphology characteristic of low-velocity impact on composite laminates, indicating that the interlaminar damage initiation and propagation are accurately captured.

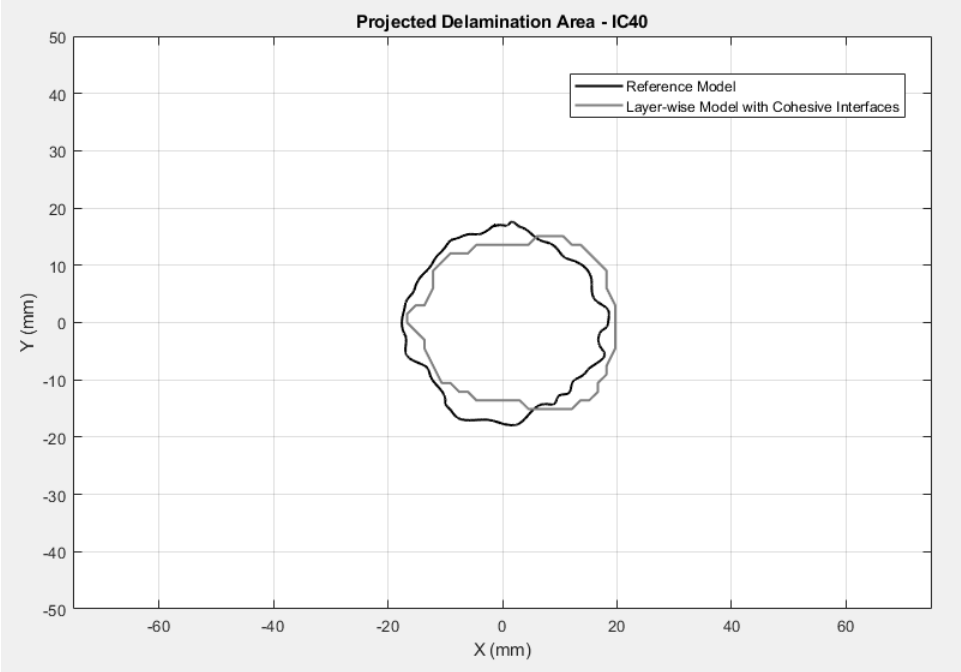


Figure 4.10 Comparison of the projected delaminated area predicted by the Layer-wise Model with Cohesive Interfaces and the analytical reference model.

Although minor local differences can be observed along the delamination boundary, the predicted damage envelope closely follows the reference solution over the entire perimeter. The numerical model predicts a slightly larger delaminated area in some regions, particularly along the lateral edges, whereas the reference solution exhibits a more irregular contour. Nevertheless, these differences remain relatively small and do not significantly affect the overall extent of the predicted damage.

The good agreement obtained is particularly significant considering the different modelling strategies adopted by both approaches. Whereas the analytical reference model employs cohesive surface interactions, the present Layer-wise Model with Cohesive Interfaces uses three-dimensional cohesive elements inserted between adjacent plies. Despite the additional mesh compatibility constraints imposed by cohesive elements, the proposed formulation is capable of reproducing the global delamination morphology with a high degree of accuracy.

This result demonstrates that the cohesive interface properties adopted in the present work provide an appropriate representation of the interlaminar fracture process. Furthermore, it indicates that the calibration performed during the model development successfully

reproduces the fracture energy required to capture the initiation and propagation of delamination under impact loading.

The accurate prediction of the projected delaminated area is particularly relevant because delamination is the dominant failure mechanism in low-velocity impact of laminated composites and one of the main quantities used to assess the severity of impact damage. Consequently, the agreement achieved in Figure 4.10 provides strong validation of the interlaminar damage formulation adopted in the Layer-wise Model with Cohesive Interfaces, even though some discrepancies remain in the prediction of the global force response and the energy dissipation.

4.4. Adaptive ERR–Cohesive Large-Element Model Results

4.4.1. Global Structural Response

The predictive capability of the Adaptive ERR–Cohesive Large-Element Model was first assessed by comparing its global structural response with the validated numerical model proposed by González et al. [8], together with the corresponding experimental results. The comparison focuses on two complementary response variables: the load–displacement relationship, which evaluates the overall structural stiffness and impact force prediction, and the internal energy evolution, which reflects the model's capability to reproduce the energy absorption mechanisms during the impact event. Achieving good agreement in both entities is essential to demonstrate that the proposed formulation can accurately capture the global mechanical behaviour, while employing a substantially coarser finite element discretisation.

Figure 4.11 presents the load–displacement response obtained with the proposed Adaptive ERR–Cohesive formulation together with the experimental measurements and the reference analytical solution [8]. Overall, the predicted response shows very good agreement with both reference curves throughout the impact event. The initial elastic region is accurately reproduced, indicating that the global stiffness of the laminate is correctly represented despite the significantly coarser mesh adopted in the present model.

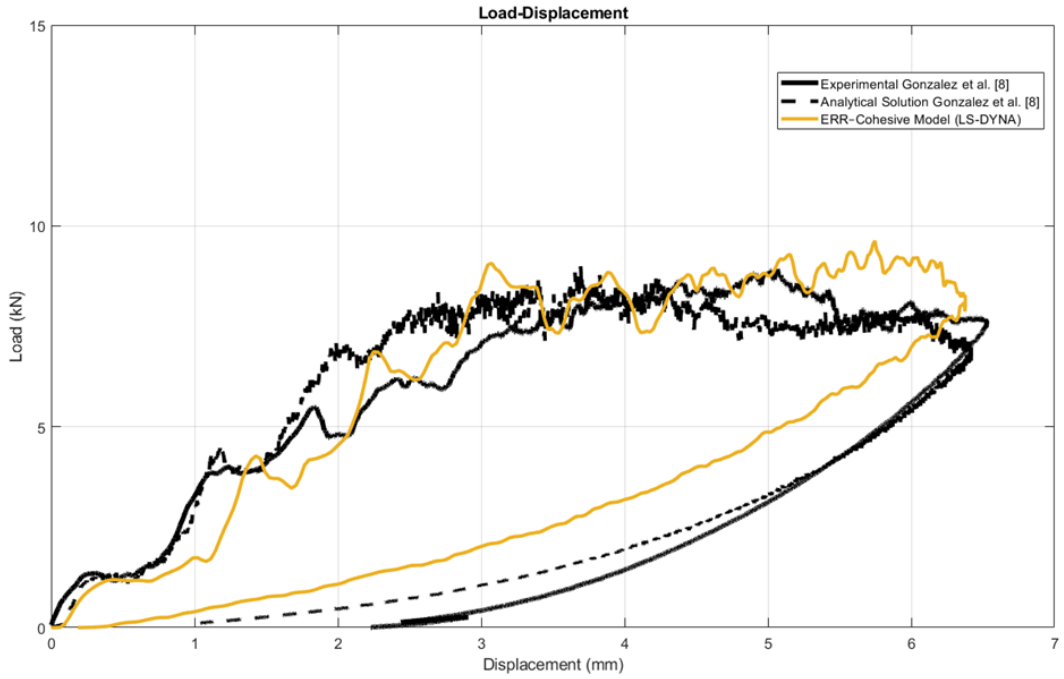


Figure 4.11 Global load–displacement response of the Adaptive ERR–Cohesive Large-Element Model compared with the experimental results and the validated reference model proposed by González et al. [8].

As the impact progresses, the numerical solution successfully captures the gradual increase in contact load and predicts a maximum load comparable to both the experimental measurements and the validated reference model. Following damage initiation, the characteristic load plateau associated with the progressive degradation of the laminate is also reproduced. Although the proposed formulation exhibits slightly larger oscillations than the reference solution, these fluctuations are typical of explicit dynamic analyses involving progressive material degradation and repeated contact interactions. Importantly, they do not affect the overall response or the predicted load level.

Minor deviations become noticeable during the final unloading stage, particularly for displacements beyond approximately 5 mm. Nevertheless, the overall evolution remains consistent with both the experimental observations and the reference simulation, demonstrating that the proposed formulation accurately reproduces the reduction in structural stiffness associated with the accumulation of intralaminar and interlaminar damage.

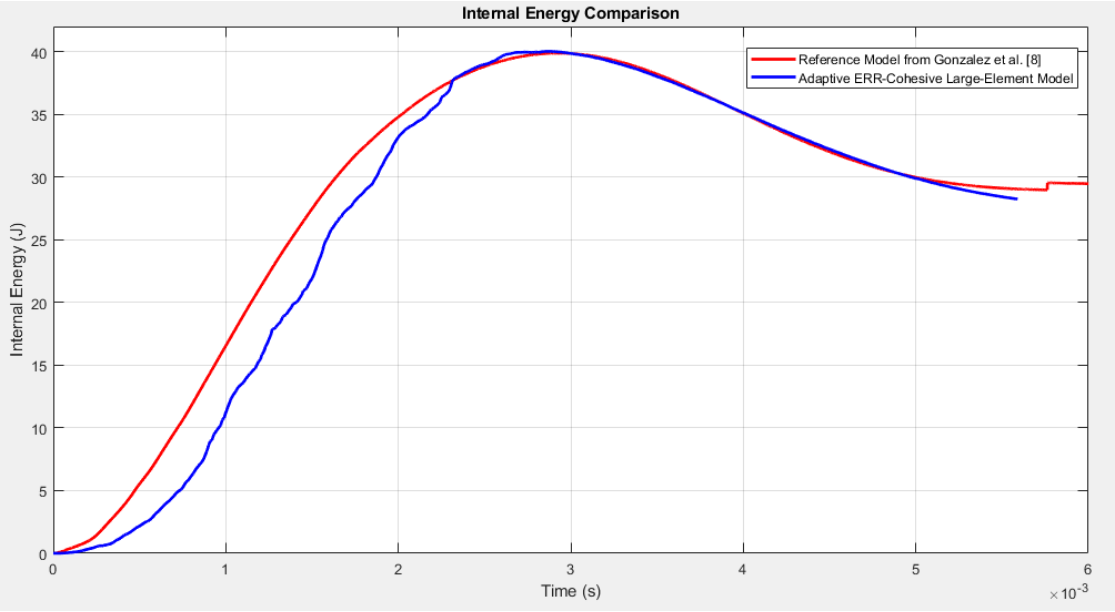


Figure 4.12 Internal energy evolution of the Adaptive ERR–Cohesive Large-Element Model compared with the validated reference model proposed by González et al. [8].

A second level of validation is provided by comparing the internal energy histories, as shown in Figure 4.12. Internal energy is a particularly relevant parameter for impact simulations, as it directly reflects the amount of energy absorbed by the structure through elastic deformation and progressive damage mechanisms.

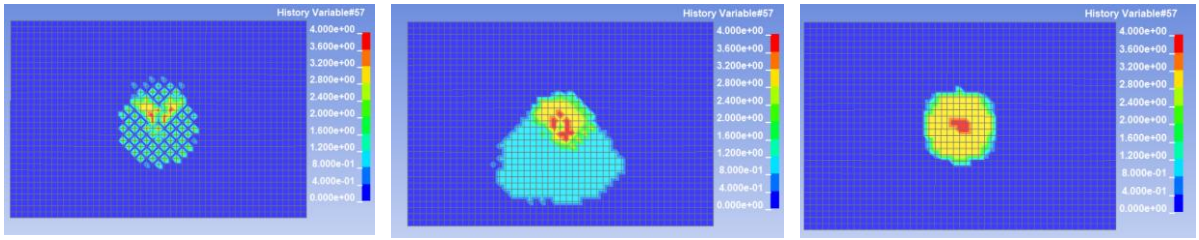
The Adaptive ERR–Cohesive model exhibits an internal energy evolution that closely follows the response of the validated reference model throughout the entire impact event. During the initial loading stage, a slightly slower increase in internal energy is observed, indicating minor differences in the onset of damage initiation. However, both models rapidly converge and reach virtually the same maximum absorbed energy of approximately 40 J, demonstrating that the proposed formulation predicts the overall energy absorption with excellent accuracy.

Following the peak value, both simulations exhibit a very similar reduction in internal energy as the impactor rebounds, with only negligible differences during the final stages of the analysis. The close agreement observed throughout both the loading and unloading phases confirms that the proposed formulation accurately reproduces the global energy dissipation mechanisms governing the impact response.

4.4.2. Hourglass Stiffness Sensitivity

During the development of the Adaptive ERR–Cohesive Large-Element Model, a sensitivity analysis was performed to evaluate the influence of the hourglass stiffness coefficient on the predicted delamination morphology. This preliminary study was carried out prior to incorporating the intralaminar progressive damage model and aimed to identify an appropriate level of numerical stabilization for the large-element formulation. Since the laminate is discretised using reduced integration solid elements, the numerical formulation is susceptible to zero-energy deformation modes, commonly referred to as hourglass modes. If these modes are not adequately controlled, they may introduce non-physical deformation patterns that directly influence the energy release rate (ERR) calculation and, consequently, the initiation and propagation of delamination.

To assess this effect, three different hourglass stiffness coefficients were investigated while maintaining all other model parameters unchanged, as shown in Figure 4.13.



(a) (b) (c)

Figure 4.13 Influence of the hourglass stiffness coefficient on the predicted delamination morphology: (a) HG = 0.01, (b) HG = 0.1 and (c) HG = 1.5.

For the lowest stabilization coefficient (HG = 0.01), the predicted delamination exhibits pronounced numerical instabilities. Instead of developing a smooth crack front, the delaminated region presents a highly irregular polygonal morphology characterised by sharp corners and oscillatory local features. Furthermore, crack propagation is clearly influenced by the underlying finite element topology, producing a mesh-induced bias in which the delamination preferentially follows the element arrangement rather than the expected physical propagation path. These observations indicate that the zero-energy deformation

modes are not sufficiently suppressed, resulting in a non-physical prediction of the interlaminar damage.

Increasing the stabilization coefficient to HG = 0.1 significantly improves the numerical behaviour. The delaminated region becomes noticeably smoother and the influence of the hourglass modes is substantially reduced. However, a preferential propagation direction can still be identified, producing an asymmetric delamination pattern that differs from the nearly circular morphology expected for a centrally impacted laminate. Although a certain degree of mesh dependency remains evident, the overall damage morphology represents a considerable improvement compared with the solution obtained using HG = 0.01.

The most stable solution obtained during this preliminary study corresponds to an hourglass stiffness coefficient of 1.5. Under this configuration, the predicted delamination develops a smooth and almost circular morphology, with no visible evidence of mesh-induced directional propagation or local numerical oscillations. The delamination front becomes significantly more uniform and closely resembles the damage morphology observed experimentally under low-velocity impact loading. Furthermore, no signs of excessive numerical stabilization, such as artificial suppression of damage growth or unrealistic localization, were observed during this initial elastic–cohesive formulation.

The comparison presented in Figure 4.13 demonstrates that the hourglass stiffness coefficient has a direct influence on the predicted interlaminar damage. Since the Adaptive ERR–Cohesive formulation determines crack initiation and propagation from the local energy release rate, any numerical instability affecting the displacement field is directly reflected in the predicted delamination morphology. Consequently, insufficient hourglass control produces non-physical crack propagation driven by numerical artefacts rather than by the actual stress field within the laminate.

Following the incorporation of the intralaminar progressive damage model, however, the numerical response of the formulation changed noticeably. The progressive degradation of the laminate naturally reduced the tendency of the model to develop hourglass-induced deformation patterns, making the solution less sensitive to the stabilization coefficient. Under

these conditions, the lower coefficient (HG = 0.1) provided a better overall agreement with both the validated reference model and the experimental response presented in Section 4.4.1. In contrast, the higher stabilization coefficient (HG = 1.5) introduced a slightly more constrained damage evolution due to the additional artificial stiffness associated with the hourglass control.

Consequently, although the preliminary sensitivity study identified HG = 1.5 as the most stable solution for the elastic–cohesive formulation, the final Adaptive ERR–Cohesive Large-Element Model presented in this dissertation employs an hourglass stiffness coefficient of 0.1.

4.4.3. Influence of the Enriched Interface Configuration

Although the Adaptive ERR–Cohesive formulation is currently limited to a maximum of five enriched interfaces, it is important to evaluate whether the selection of these interfaces influences the predicted delamination response. Since the energy release rate is evaluated only at the enriched interfaces, an inappropriate distribution through the laminate thickness could potentially affect the initiation and propagation of interlaminar damage. However, following the incorporation of the intralaminar progressive damage model, the redistribution of stresses and strain energy within the laminate is expected to reduce this dependency, resulting in a more robust formulation.

Figure 4.14 compares the projected delamination areas obtained using four different enriched interface configurations. The investigated cases correspond to the interface sets 136911, 23456, 45678, and 246810, which represent different through-thickness distributions of the adaptive enrichment.

Overall, the four configurations produce remarkably similar delamination patterns. The predicted delaminated areas exhibit nearly identical dimensions, crack propagation directions, and overall morphology, with only minor local differences along the delamination front. In all cases, the damage remains approximately circular, which is consistent with the expected behaviour of a centrally impacted laminate under low-velocity impact loading.

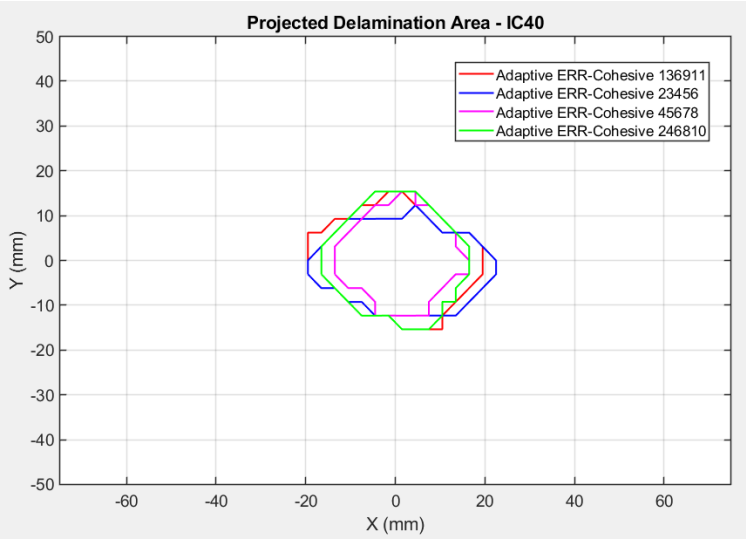


Figure 4.14 Projected delamination area predicted using four different enriched interface configurations.

The small discrepancies observed between the different configurations are mainly restricted to local variations along the delamination boundary. These differences do not significantly modify either the projected damaged area or the global delamination morphology, indicating that the predicted interlaminar fracture process is largely independent of the selected enriched interfaces.

This behaviour differs from that observed during the early stages of the model development, where the formulation without intralaminar progressive damage exhibited a much stronger sensitivity to the interface configuration. Once the progressive degradation of the plies is incorporated, the stresses and strain energy are redistributed more realistically throughout the laminate thickness. As a result, the initiation and propagation of delamination are governed primarily by the structural response of the laminate rather than by the exact location of the enriched interfaces.

These results demonstrate that the Adaptive ERR–Cohesive formulation is highly robust with respect to the selection of enriched interfaces once intralaminar progressive damage is considered. This represents an important practical advantage, as accurate delamination predictions can be obtained without requiring the identification of a unique optimal enrichment strategy for each laminate configuration. Consequently, the proposed

methodology offers greater flexibility for practical engineering applications while maintaining the computational efficiency associated with the adaptive large-element formulation.

4.4.4. Delamination Pattern Validation

Although the global structural response provides an important measure of the accuracy of the proposed formulation, the principal objective of the Adaptive ERR–Cohesive Large-Element Model is the prediction of delamination. Therefore, the final stage of the validation consists of comparing the projected delamination area predicted by the proposed formulation with that obtained using the validated layer-wise reference model developed by González et al. [8].

Figure 4.15 compares the projected delamination area predicted by the Adaptive ERR–Cohesive formulation with the corresponding reference solution. Overall, all four enriched interface configurations reproduce the characteristic delamination morphology observed in the validated model. Despite the different distributions of enriched interfaces through the laminate thickness, the predicted delamination remains approximately circular and exhibits a projected area that closely matches the reference solution.

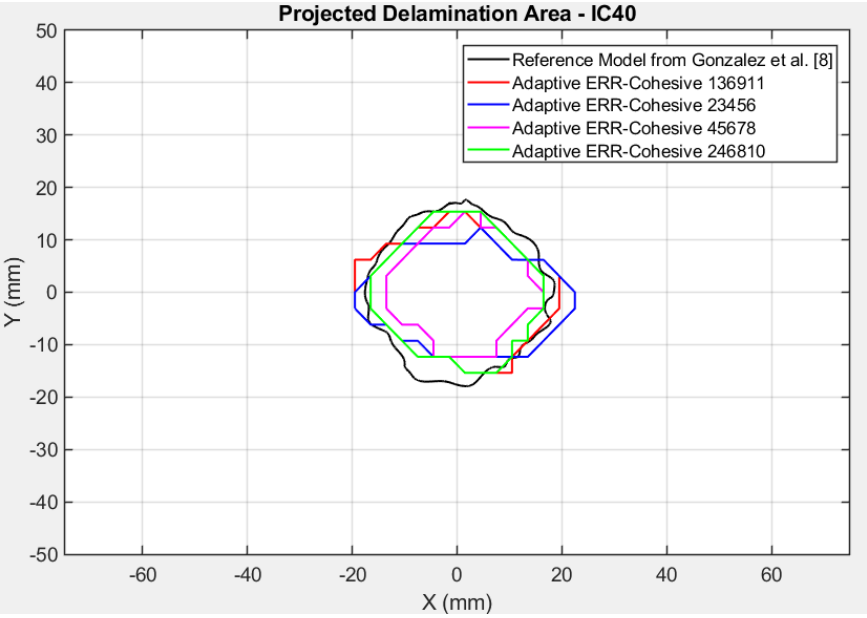


Figure 4.15 Comparison of the projected delamination area predicted by the Adaptive ERR–Cohesive Large-Element Model using different enriched interface configurations and the validated reference model proposed by González et al. [8].

Small local discrepancies are observed along the delamination front. In particular, the Adaptive ERR–Cohesive formulation predicts a polygonal boundary, whereas the reference model presents a smoother contour. This behaviour is primarily attributed to the coarse finite element discretisation employed by the adaptive formulation, where the crack front is constrained by the element size. Nevertheless, the overall dimensions and spatial distribution of the delaminated region remain in good agreement with the reference model.

An important observation is that all enriched interface configurations produce nearly identical delamination patterns, reinforcing the conclusions presented in the previous section. The limited influence of the interface distribution demonstrates that, once intralaminar progressive damage is incorporated, the predicted interlaminar fracture process becomes largely independent of the selected enrichment strategy. Consequently, the global delamination morphology is governed by the structural response of the laminate rather than by the specific location of the enriched interfaces.

Although the reference layer-wise formulation provides a smoother representation of the crack front due to its finer mesh discretisation, the Adaptive ERR–Cohesive model successfully captures the dominant characteristics of the delamination process while employing a substantially coarser mesh and only a limited number of enriched interfaces. This represents a significant practical advantage, as it enables an accurate prediction of the projected delaminated area while considerably reducing the computational cost of the analysis.

Overall, the agreement obtained in terms of load–displacement response, internal energy evolution and projected delamination area demonstrates that the proposed Adaptive ERR–Cohesive Large-Element Model provides a reliable and computationally efficient alternative to conventional layer-wise impact models for predicting low-velocity impact damage in composite laminates.

4.5. Comparative Assessment of the Two Modelling Approaches

4.5.1. Validated aspects

The results presented throughout this chapter demonstrate that both numerical approaches are capable of reproducing the principal damage mechanisms associated with low-velocity impact on composite laminates, although they achieve this using fundamentally different modelling strategies.

The Layer-wise Model with Cohesive Interfaces provides a detailed representation of the impact event by explicitly modelling each ply and every interlaminar interface. This modelling strategy accurately reproduces the projected delaminated area while simultaneously capturing the evolution of both interlaminar and intralaminar damage mechanisms. The use of continuum shell elements together with cohesive interfaces throughout the laminate thickness enables a detailed description of damage initiation and propagation, making this approach particularly suitable for investigating local failure mechanisms.

The Adaptive ERR–Cohesive Large-Element Model, despite employing a substantially coarser mesh and enriching only five interfaces, successfully reproduces the global structural response of the validated reference model. Excellent agreement is achieved for both the load–displacement response and the internal energy evolution, demonstrating that the adaptive formulation accurately captures the global stiffness, peak load and energy absorption characteristics of the impacted laminate. Furthermore, the incorporation of the intralaminar progressive damage model enables the formulation to reproduce progressive fibre degradation and nonlinear shear behaviour, providing a significantly more realistic representation of the impact event than the previous elastic implementation.

In addition to the accurate prediction of the global response, the Adaptive ERR–Cohesive formulation also reproduces the projected delaminated area and the overall delamination morphology with good agreement. Although the coarser finite element discretisation produces a more polygonal crack front than the layer-wise reference model, the predicted damage extent and overall propagation pattern remain consistent with the validated solution.

Moreover, the sensitivity study demonstrated that, once intralaminar progressive damage is incorporated, the predicted delamination becomes largely independent of the selected enriched interface configuration. This represents an important improvement over the preliminary elastic formulation, where the interface selection had a much greater influence on the predicted damage.

Overall, the results confirm that the Adaptive ERR–Cohesive methodology preserves the predictive capability of conventional layer-wise impact models while significantly reducing the numerical complexity of the simulation.

4.5.2. Limitations

Although both numerical approaches provide an accurate prediction of the impact response, several limitations remain that should be addressed in future developments.

For the Layer-wise Model with Cohesive Interfaces, the principal limitation is associated with the computational cost required to explicitly model every ply and every interlaminar interface. Although this modelling strategy provides a highly detailed representation of the damage mechanisms, it requires a fine through-thickness discretisation together with matching meshes between adjacent plies. Consequently, the ±45° plies cannot be independently discretised according to their material directions, which may influence the local stress distribution and the prediction of intralaminar damage. Furthermore, the computational expense of the layer-wise formulation limits its applicability to large composite structures or analyses requiring multiple design iterations.

The Adaptive ERR–Cohesive Large-Element Model substantially reduces the computational cost while maintaining good agreement with the validated reference solution. However, the current implementation remains limited to a maximum of five enriched interfaces, which must be defined prior to the simulation. Although the results presented in Section 4.4 demonstrate that the incorporation of intralaminar progressive damage significantly reduces the sensitivity to the selected interface configuration, a fully adaptive enrichment strategy capable of

activating interfaces automatically during the analysis would further improve the generality and robustness of the methodology.

In addition, the present validation has been performed for a single laminate configuration subjected to a low-velocity impact event. Further assessment under different stacking sequences, laminate thicknesses, impact energies and boundary conditions would provide a more comprehensive evaluation of the proposed methodology and establish its applicability across a broader range of composite impact problems.

4.5.3. Suitability for large-scale structures

Although both modelling approaches provide an accurate prediction of the projected delaminated area, their computational requirements differ considerably. The simulation times measured during the present study are summarised in Table 4.1.

Table 4.1 Required simulation time for each model

Model	Simulation time
Layer-wise Model with Cohesive Interfaces	4–5 h
Adaptive ERR–Cohesive Large-Element Model	~40 min

Using the average simulation times obtained in this work (4.5 h and 40 min, respectively), the Adaptive ERR–Cohesive Large-Element Model reduces the computational time by approximately 85%, making it almost seven times faster than the Layer-wise Model with Cohesive Interfaces.

This significant reduction is achieved while maintaining excellent agreement with the validated reference model in terms of the load–displacement response, internal energy evolution, and projected delamination area. These results demonstrate that the adaptive methodology successfully preserves the predictive capability of conventional layer-wise modelling strategies while substantially reducing the computational cost. Such an improvement is particularly relevant for the simulation of large composite structures, where

conventional layer-wise approaches rapidly become prohibitively expensive due to the large number of degrees of freedom required.

The reduced computational cost also makes the Adaptive ERR–Cohesive formulation particularly attractive for engineering applications involving multiple simulations, such as design optimisation, parametric studies and virtual testing, where the use of conventional layer-wise models would often be impractical. By combining a coarse finite element discretisation with a physically based adaptive delamination formulation, the proposed methodology provides an effective compromise between computational efficiency and predictive accuracy.

Overall, the results presented throughout this chapter demonstrate that the Adaptive ERR–Cohesive Large-Element Model constitutes a reliable and computationally efficient alternative to conventional layer-wise impact models. Despite employing a substantially coarser mesh and enriching only a limited number of interfaces, the proposed formulation accurately reproduces the global structural response, energy absorption characteristics and delamination morphology of the validated reference model while reducing the computational time by approximately 85%. These characteristics make the methodology particularly suitable for the analysis of large composite structures, where computational efficiency is essential without compromising the accuracy of impact damage prediction.

THIS PAGE WAS INTENTIONALLY LEFT BLANK

5. CONCLUSIONS

5.1. Summary of the main findings

The primary objective of this dissertation was to develop and validate an adaptive Energy Release Rate (ERR)–cohesive formulation capable of accurately predicting low-velocity impact damage in composite laminates while significantly reducing the computational cost associated with conventional layer-wise modelling strategies. The results presented throughout this work demonstrate that this objective has been successfully achieved.

To accomplish this, two different numerical modelling approaches were developed and investigated. The first consisted of a Layer-wise Model with Cohesive Interfaces implemented in Abaqus®, which served as a high-fidelity reference model. The second was the proposed Adaptive ERR–Cohesive Large-Element Model implemented in LS-DYNA®, which combines a coarse finite element discretisation with an adaptive interlaminar fracture formulation and a progressive intralaminar damage model.

The Layer-wise Model with Cohesive Interfaces successfully reproduced the principal damage mechanisms associated with low-velocity impact loading. By explicitly modelling every ply and every interlaminar interface, the formulation provided an accurate prediction of the projected delaminated area together with a detailed representation of both interlaminar and intralaminar damage evolution. Consequently, this model constituted a reliable benchmark for assessing the performance of the proposed adaptive methodology.

The principal contribution of this dissertation is the successful development and validation of the Adaptive ERR–Cohesive Large-Element Model. Despite enriching only five interfaces and employing a substantially coarser finite element mesh, the proposed methodology accurately reproduced the global structural response of the validated reference model. Excellent agreement was obtained for the load–displacement response, internal energy evolution and projected delamination area, demonstrating that the adaptive formulation successfully

captures both the global mechanical behaviour and the dominant damage mechanisms governing low-velocity impact.

The incorporation of the intralaminar progressive damage formulation represented a key improvement to the adaptive methodology. In addition to enabling the prediction of progressive fibre degradation and nonlinear shear behaviour, the enhanced formulation significantly reduced the sensitivity of the model to the selected enriched interface configuration. Consequently, the predicted delamination became largely independent of the specific placement of the enriched interfaces, demonstrating that the proposed methodology is robust and suitable for practical engineering applications.

The numerical sensitivity analyses also confirmed the importance of appropriate numerical stabilisation. The hourglass stiffness study demonstrated that adequate suppression of zero-energy deformation modes is essential to obtain physically meaningful crack propagation and reliable delamination predictions. Once the progressive damage formulation was incorporated, however, the model exhibited a stable and consistent response while maintaining excellent agreement with the validated reference solution.

Perhaps the most significant outcome of this research is that the proposed Adaptive ERR–Cohesive methodology preserves the predictive capability of conventional layer-wise impact models while substantially reducing their computational cost. The simulation time was reduced by approximately 85%, from 4–5 hours for the Layer-wise Model with Cohesive Interfaces to approximately 40 minutes for the Adaptive ERR–Cohesive Large-Element Model, without compromising the accuracy of the global structural response or the predicted damage morphology.

The work presented in this dissertation demonstrates that the Adaptive ERR–Cohesive Large-Element Model constitutes a validated, robust and computationally efficient methodology for the simulation of low-velocity impact damage in composite laminates. By accurately reproducing the global structural response, energy absorption characteristics and delamination morphology while reducing the computational cost by approximately 85%, the proposed formulation bridges the gap between the predictive capability of conventional layer-

wise models and the computational efficiency required for the analysis of large composite structures.

5.2. Research Objectives Achievement

The research objectives established at the beginning of this dissertation have been successfully achieved.

The first objective, consisting of implementing the Adaptive ERR–Cohesive methodology within a finite element framework suitable for the analysis of large composite structures, was successfully accomplished. The proposed formulation was implemented in LS-DYNA and integrated with a progressive intralaminar damage model, resulting in a stable and robust numerical framework capable of simulating low-velocity impact events using a substantially reduced finite element discretisation.

The second objective was to reproduce the impact model proposed by González et al. [8] using a Layer-wise Model with Cohesive Interfaces based exclusively on standard Abaqus® material models. Despite replacing the proprietary constitutive implementation employed in the reference work, the developed model successfully reproduced the principal damage mechanisms associated with low-velocity impact, providing an accurate prediction of the projected delaminated area together with a detailed representation of both interlaminar and intralaminar damage. Consequently, the model constituted a reliable benchmark for validating the proposed adaptive methodology.

The third objective involved evaluating the predictive capability of the Adaptive ERR–Cohesive Large-Element Model. This objective was successfully fulfilled. Despite employing only five enriched interfaces and a substantially coarser finite element mesh, the adaptive formulation accurately reproduced the validated reference model in terms of the load–displacement response, internal energy evolution, and projected delamination area. Furthermore, the incorporation of the progressive intralaminar damage formulation significantly improved the physical representation of the impact event while reducing the sensitivity of the predicted

delamination to the selected enriched interface configuration, demonstrating the robustness of the proposed methodology.

The final objective was to assess the computational efficiency of the adaptive formulation as an alternative to conventional layer-wise modelling strategies. The results demonstrated that the proposed methodology reduced the simulation time by approximately 85%, decreasing the computational time from approximately 4–5 hours to approximately 40 minutes, while maintaining excellent agreement with the validated reference model. This reduction in computational cost was achieved without compromising the prediction of the global structural response, energy absorption characteristics or delamination morphology.

The achievement of these objectives confirms that the proposed Adaptive ERR–Cohesive Large-Element Model fulfils the aims established for this research. The developed methodology combines the predictive capability of conventional layer-wise impact models with a substantial reduction in computational cost, providing an accurate, robust and computationally efficient framework for the simulation of low-velocity impact damage in composite laminates and establishing a solid foundation for its future application to large composite structures.

5.3. Limitations and Future Work

Although the objectives of this dissertation have been successfully achieved, several limitations remain and provide clear directions for future research.

The principal limitation of the Layer-wise Model with Cohesive Interfaces is associated with its computational cost and modelling requirements. The explicit representation of every ply and every cohesive interface requires a fine through-thickness discretisation and matching meshes between adjacent plies, making the methodology computationally demanding for large composite structures. Future developments should therefore focus on improving the efficiency of conventional layer-wise formulations while maintaining their high level of predictive accuracy.

For the Adaptive ERR–Cohesive Large-Element Model, the current implementation remains limited to a maximum of five enriched interfaces, which must be specified before the analysis. Although the results of this dissertation demonstrate that the incorporation of progressive intralaminar damage substantially reduces the sensitivity to the selected interface configuration, the enrichment process is not yet fully adaptive. Future work should therefore focus on developing an automatic enrichment strategy capable of identifying and activating the most critical interfaces during the simulation according to the evolving stress and energy distribution within the laminate.

Another important aspect concerns the general applicability of the proposed methodology. The present work has been validated for a representative low-velocity impact case using a single laminate configuration and impact energy. Extending the validation to different stacking sequences, laminate thicknesses, impact energies and boundary conditions would provide a broader assessment of the robustness and predictive capability of the adaptive formulation.

From a computational perspective, an important direction for future research is the application of the proposed methodology to large and geometrically complex composite structures, where the computational advantages of the Adaptive ERR–Cohesive formulation are expected to become even more significant. Such applications would provide a more representative assessment of the methodology under realistic engineering conditions and further demonstrate its suitability for industrial-scale analyses.

Finally, the encouraging results obtained in this dissertation suggest that the proposed Adaptive ERR–Cohesive methodology could serve as a foundation for future developments in adaptive composite damage modelling. The combination of accurate prediction of the global structural response, interlaminar delamination and progressive intralaminar damage with a substantially reduced computational cost highlights the potential of the methodology for the efficient simulation of impact damage in large composite structures. Further developments towards fully adaptive enrichment algorithms and broader experimental validation would represent the next logical step in advancing the methodology towards routine engineering applications.

REFERENCES

[1] P. K. Mallick, Fiber-Reinforced Composites: Materials, Manufacturing, and Design, 3rd ed. Boca Raton, FL, USA: CRC Press, 2007.

[2] D. Hull and T. W. Clyne, An Introduction to Composite Materials, 2nd ed. Cambridge, U.K.: Cambridge University Press, 1996.

[3] L. Tong, A. P. Mouritz and M. K. Bannister, 3D Fibre Reinforced Polymer Composites. Oxford, U.K.: Elsevier, 2002.

[4] A. P. Mouritz and A. G. Gibson, Fire Properties of Polymer Composite Materials. Dordrecht, Netherlands: Springer, 2006.

[5] A. Turon, P. P. Camanho, J. Costa and C. G. Dávila, "An engineering solution for mesh size effects in the simulation of delamination using cohesive zone models," Engineering Fracture Mechanics, vol. 74, no. 10, pp. 1665–1682, 2007.

[6] R. Krueger, "The virtual crack closure technique: History, approach and applications," Applied Mechanics Reviews, vol. 57, no. 2, pp. 109–143, 2004.

[7] P. P. Camanho, C. G. Dávila and M. F. de Moura, "Numerical simulation of mixed-mode progressive delamination in composite materials," Journal of Composite Materials, vol. 37, no. 16, pp. 1415–1438, 2003.

[8] E. V. González, P. Maimí, E. Martín-Santos, A. Soto, P. Cruz, F. M. de la Escalera and J. R. Sainz de Aja, "Simulating drop-weight impact and compression after impact tests on composite laminates using conventional shell finite elements," International Journal of Solids and Structures, vol. 144–145, pp. 230–247, 2018.

[9] P. P. Camanho, C. G. Dávila, S. T. Pinho, L. Iannucci and P. Robinson, "Prediction of in situ strengths and matrix cracking in composites under transverse tension and in-plane shear," Composites Part A: Applied Science and Manufacturing, vol. 37, no. 2, pp. 165–176, 2006.

[10] P. M. Daniel, J. Främby, M. Fagerström and P. Maimí, "An efficient ERR-cohesive method for the modelling of delamination propagation with large elements," Composites Part A: Applied Science and Manufacturing, vol. 167, 2023, Art. no. 107423.

[11] P. M. Daniel, J. Främby, M. Fagerström and P. Maimí, "A method for modelling arbitrarily shaped delamination fronts with large and distorted elements," Engineering Fracture Mechanics, vol. 306, 2024, Art. no. 110193.

[12] A. A. Griffith, "The phenomena of rupture and flow in solids," Philosophical Transactions of the Royal Society A, vol. 221, pp. 163–198, 1921.

[13] M. L. Benzeggagh and M. Kenane, "Measurement of mixed-mode delamination fracture toughness of unidirectional glass/epoxy composites with mixed-mode bending apparatus," Composites Science and Technology, vol. 56, no. 4, pp. 439–449, 1996.

[14] E. F. Rybicki and M. F. Kanninen, “A finite element calculation of stress intensity factors by a modified crack closure integral,” Engineering Fracture Mechanics, vol. 9, no. 4, pp. 931–938, 1977.
[15] D. Xie, A. M. Waas, R. Shahwan and V. C. Boay, “Computation of strain energy release rates for discrete crack growth in mixed-mode delamination problems,” Composite Structures / related works on arbitrary delamination fronts in regular meshes.
[16] Daniel, P. M. (2025). A strategy for efficient modelling of composite delamination in large structures (Doctoral dissertation). Universitat de Girona, Girona, Spain.
[17] D. Xie, S. B. Biggers, Strain energy release rate calculation for a moving delamination front of arbitrary shape based on the virtual crack closure technique. part i: Formulation and validation, Engineering Fracture Mechanics 73 (2006) 771–785.
[18] D. Xie, S. B. Biggers, Strain energy release rate calculation for a moving delamination front of arbitrary shape based on the virtual crack closure technique. part ii: Sensitivity study on modeling details, Engineering Fracture Mechanics 73 (2006) 786–801.
[19] Y.-P. Liu, C.-Y. Chen, G.-Q. Li, A modified zigzag approach to approximate moving crack front with arbitrary shape, Engineering Fracture Mechanics 78 (2011) 234–251.
[20] Y.-P. Liu, G.-Q. Li, C.-Y. Chen, Crack growth simulation for arbitrarily shaped cracks based on the virtual crack closure technique, International Journal of Fracture 185 (2014) 1–15.
[21] M. Marjanovi´c, G. Meschke, D. Vuksanovi´c, A finite element model for propagating delamination in laminated composite plates based on the virtual crack closure method, Composite Structures 150 (2016) 8–19.
[22] A. C. Orifici, R. S. Thomson, R. Degenhardt, C. Bisagni, J. Bayandor, Development of a finite-element analysis methodology for the propagation of delaminations in composite structures, Mechanics of Composite Materials 43 (2007) 9–28.
[23] L. M. Martulli, A. Bernasconi, An efficient and versatile use of the vcct for composites delamination growth under fatigue loadings in 3d numerical analysis: the sequential static fatigue algorithm, International Journal of Fatigue 170 (2023) 107493.
[24] M. W. McElroy, R. Gutkin, M. Pankow, Interaction of delaminations and matrix cracks in a cfrp plate, part ii: Simulation using an enriched shell finite element model, Composites Part A: Applied Science and Manufacturing 103 (2017) 252–262.
[25] ANSYS Inc., ANSYS Mechanical APDL Theory Reference, Release 18.2, Canonsburg, PA, USA, 2018. Available: https://www.mm.bme.hu/~gyebro/files/ans_help_v182/ans_thry/thy_mat11.html
[26] A. Turon, P. P. Camanho, J. Costa and J. Renart, “Accurate simulation of delamination growth under mixed-mode loading using cohesive elements: Definition of interlaminar strengths and elastic stiffness,” Composite Structures, vol. 92, no. 8, pp. 1857–1864, 2010.
[27] C. Sarrado, A. Turon, J. Renart and I. Urresti, “Assessment of energy dissipation during mixed-mode delamination growth using cohesive zone models,” Composites Part A: Applied Science and Manufacturing, vol. 43, no. 11, pp. 2128–2136, 2012.

[28] A. Turon, E. V. González, C. Sarrado, G. Guillamet and P. Maimí, “Accurate simulation of delamination under mixed-mode loading using a cohesive model with a mode-dependent penalty stiffness,” Composite Structures, vol. 184, pp. 506–511, 2018.
[29] Martín-Santos, E., Maimí, P., González, E.V., Cruz, P., 2014. A continuum constitutive model for the simulation of fabric-reinforced composites. Composite Structures, 111, pp. 122–129. https://doi.org/10.1016/j.compstruct.2013.12.024